EFFECT OF SURFACE MODIFICATION WITH ELECTROSPUN NANOFIBERS ON THE PERFORMANCE OF THE ULTRAFILTRATION MEMBRANE

By:

Ladan Zoka

Master of Applied Science Thesis

Submitted to the School of Graduate Studies and Research under the supervision of

Dr. Takeshi Matsuura and Dr. Roberto M. Narbaitz

In partial fulfilment of the requirement for the degree of Master of Applied Science in Environmental Engineering

The degree is offered under Ottawa- Carleton Institute for Environmental Engineering
Department of Civil Engineering at University of Ottawa

Ottawa, Ontario

Canada K1N 6N5

ABSTRACT

Membrane surface modification is often utilized to combat membrane fouling, i.e., the deterioration of membrane performance with time. Among many modification methods, the effect of coating the surface of a commercial membrane with electrospun nanofibers on the membrane performance has received little attention.

In this work, a commercial polyethersulfone (PES) ultrafiltration membrane was modified by electrospinning PVDF hydrophobic nanofibers for different time periods, i.e., 25min, 125min, and 250min, and its effect on the filtration performance was investigated. It was found that coating with the electrospun nanofiber layer enhanced the pure water permeation (PWP) flux. While the fouling of electrospun PES (EPES) membranes was more severe when they filtered Ottawa River (OR) Water or protein solutions, their final flux was still higher than that of the PES membrane. The membranes were further characterized by scanning electron microscopy (SEM), contact angle measurement and pore size and pore size distribution. The relationship between these characteristics and the membrane performance was discussed.

I dedicate this study to:

My father`s soul,

My mom,

Pedram and

Tanaz

ACKNOWLEDGEMENTS

I would like to express my gratitude to my supervisors Dr. Takeshi Matsuura and Dr. Roberto Narbaitz for their continuous support, guidance, patience, enthusiasm, and immense knowledge during all the testing and writing my thesis. This work would not have been possible without them.

I would also like to thank Dr. Dipak Rana from the Department of Chemical and Biochemical Engineering for his support and advice. I would like to thank Louis Tremblay, the chemical engineering technician, for his help and recommendations. Also, I would like my friend and lab co- worker Johnson Efome for teaching me how to use the electrospinning equipment.

I would like to thank my dear friends Bingjie Xu and Pablo Gonzalez Galvis for their help, support, and encouragement. We were Dr. Narbaitz's students and Bingjie was the first friend that I met since the beginning of the master's program. Also, I would like to thank Patrick D'Aoust, environmental engineering lab technician, and Neda Arabgol as my friends, classmates, office mates, and for their help and advice. My other friends in the same office: Nour Al- ghuasian, Kellie Boyle, and Maha Dabas always supported me. Thanks for all those precious times of laughing, chating, and crying we spent together.

And at the end I would like to thank my angels, my parents. I need to give an additional thanks to my dear husband Pedram Fouladirad and my pretty and lovely daughter Tanaz Fouladirad for their support, love, understanding, inspiration, and encouragement. Thanks to my dear sister Rana for her support and advice in this journey. Thanks to my brother, Mohammad, for his support from far away.

TABLE OF CONTENTS

List of Tables

List of Figures

ABBREVIATIONS

BSA	Bovine serum albumin
CA	Cellulose acetate
CS	Chitosan
D	Dialysis
DMAc	Dimethylacetamide
DW	Distilled water
DOC	Dissolved organic carbon
EDTA	Ethylenediaminetetraacetic acid
EfoM	Effluent organic matter
ENMs	Electrospun nanofiber membranes
EPES	Electrospun polyethersulfone membrane
ESP	Extracellular polymeric substances
FA	Fulvic acid
$Fe(OH)_3$	Ferric hydroxide
GS	Gas separation
HA	Humic acids
HPO	Hydrophobic NOM fraction
ID	Inner diameter
IPA	Isopropyl alcohol
LiCl	Lithium chloride
$LiNO_3$	Lithium nitrate

MC	Methylcellulose
MF	Microfiltration
MWCO	Molecular weight cut off
NF	Nanofiltration
NMP	N-methylpyrrolidone
NOM	Natural organic matter
OD	Outer diameter
OR	Ottawa River
PAN	Polyacrylonitrile
PEO	Polyethylene oxide
PES	Polyethersulfone
PET	Polyethylene terephthalate
PI	Polyimide
PLA	Poly (lactic acid)
PS	Polystyrene
PSF	Polysulfone
PV	Pervaporation
PVA	Polyvinyl alcohol
PVC	Polyvinyl chloride
PVP	Polyvinylpyrrolidone
PWP	Pure water permeate
SEM	Scanning electron microscopy
Sepa CF	Sepa cross-flow membrane cell

SMM Surface modifying macromolecules

SMPS Soluble microbial products

SUVA Specific UV absorption

TFL Thin-film-layer

Tm Melting point temperature

TMP Transmembrane pressure

UF Ultrafiltration

UV Ultraviolet absorbance

GLOSSARY

LMH	Unit for flux (L m^{-2} h^{-1})
KDa	Kilo daltons
J	Permeate flux: flow per unit area (L m^{-2} h^{-1})
R	Solute separation
C_p	Permeate concentration (mg L^{-1})
C_f	Feed concentration (mg L^{-1})
Abs	Unitless
ε	Molar absorptivity (L mol^{-1} cm^{-1})
b	Length of the sample (cm)
c	Concentration of the compound in solution (mol L^{-1})
I_0	Transmitted intensity of reference blank
I	Transmitted intensity of sample
J_{PWP}	Pure water permeate flux (L m^{-2} h^{-1})
J_{BSA}	Bovine serum albumin solution flux (L m^{-2} h^{-1})
J_{w0}	The first pure water flux (L m^{-2} h^{-1})
J_{w1}	The last pure water flux (L m^{-2} h^{-1}) before the fouling experiment
J_{w2}	The last pure water flux (L m^{-2} h^{-1}) of post fouling experiment
J_p	The last flux (L m^{-2} h^{-1}) with OR Water (i.e., the fouling test)
R_{irr}	Fractional flux reduction due to irreversible fouling based on J_{w1}

R_{rev}	Fractional flux reduction due to reversible fouling based on J_{w1}
Rtotal	Fractional flux reduction due to both irreversible and reversible fouling based on J_{w1}
Compaction	Fractional flux reduction by compaction based on J_{w0}
T	Temperature
η	Viscosity of water (Pa s)
M	Molecular weight (g mol^{-1})
D	Diffusivity (m^2 s^{-1})
K	Boltzmann constant (1.38 x 10^{-23} J K^{-1})
V	Permeate volume (L)
t	Time (h)
A	Effective membrane area (m^2)

CHAPTER 1

INTRODUCTION

Providing sustainable supplies of clean water and energy, two interrelated resources at affordable costs, is one of the greatest challenges of 21st century. Membrane technology has been playing an important role as a technology for water production and energy saving. Membrane processes are now extensively used in drinking water treatment, waste water reuse, seawater desalination, dialysis, chemical separation processes, etc. However, there is a necessity to develop membranes with higher fluxes, higher selectivity, lower vulnerability to different types of fouling and chemical environments, especially chlorine which is used extensively in drinking water treatment (Geise, et al., 2010).

One of the main concerns with membrane separation processes is the accumulation of solids and solutes on top of the membrane surface, or within the membrane pores. This phenomenon is called fouling, which results in a reduction of the flux (the water production rate per unit membrane area) in constant pressure systems and an increase in the pressure drop in steady flux systems. Fouling is combated by operational means, such as backwashing and chemical cleaning. Even with these precautions fouling is inevitable and may lead to premature membrane replacement. Modification of the membrane surface can be achieved either chemically or physically. Physical modification includes morphological modifications (Jamshidi, et al., 2013).

Electrospinning efficiently produces continuous ultrafine polymer fibers on either polymer or molten solutions (Bjorge, et al., 2010). Huang et al. 2003 have claimed, electrospinning is one of the most successful methods that can be used in nanofiber production. And as such, electrospinning has the potential of being a technique to modify the surface of membranes by adding layers of nanofibers to the membrane surface. Numerous studies (Yoon et al., 2009; Wang et al., 2012; Khamforoush et al., 2015; Wang et al., 2017; Dobosez et al., 2017) have shown that porous membrane support material coated with electrospun layers can yield high flux membranes.

The objective of this work is to investigate the effects of coating the surface of a commercial membrane. It is in contrast with most of the earlier studies where the support material or the base membranes were laboratory made. To this end, a commercial PES ultrafiltration membrane, known as a membrane of high mechanical strength, was chosen to be coated with nanofiber layers of electrospun PVDF, known as a chlorine resistant and mechanically strong polymer (www.porex.com/technologies/materials/porous-plastics/polyvinylidene-fluoride/). The filtration performance of the electrospun coated membrane will be compared with the pristine PES membrane.

CHAPTER 2

LITERATURE REVIEW

This chapter introduces membrane separation process, types of available membranes and their characteristics, membrane fouling, followed by a discussion of different membrane making processes and modification approaches to minimize fouling.

2.1 Membranes

Selective mass transport is permitted by a thin barrier known as a membrane. A wide variety of organic polymers and liquids and also inorganic carbons and zeolites can be used in membrane fabrication (Pinnau & Freeman, 2000). Presently, polymers are used for the fabrication of most commercial membranes. The most common polymer membranes are listed in Table 2.1 on the following page.

Table 2.1 Common polymeric commercial membranes (Pinnau & Freeman, 2000)

Membrane material	Membrane process*
Cellulose regenerated	D, UF, MF
Cellulose acetate	GS, RO, D, UF, MF
Polyamide	RO, NF, D, UF, MF
Polysulfone	GS, UF, MF
Poly (ether sulfone)	UF, MF
Polycarbonate	GS, D, UF, MF
Poly (ether imide)	UF, MF
Poly (vinylidene fluoride)	UF, MF
Polyacrylonitrile	D, UF, MF
Poly (methyl methacrylate)	D, UF

*MF= microfiltration; UF= ultrafiltration; NF= nanofiltration; D= dialysis;

PV= pervaporation; GS= gas separation

In general, the material and morphology of the membrane control the properties and performance of the membranes. Pinnau (1994) claimed that a membrane with at least the following characteristics is useful in an industrial separation process:

- High flux,

- High selectivity (rejection),

- Mechanical stability,

- Tolerance to all feed stream components (fouling resistance),

- Tolerance to temperature variations,

- Manufacturing reproducibility,(Buonomenna, Choi, Galiano, & Drioli, 2011)

- Low manufacturing cost, and

- Ability to be packaged into high surface area modules.

Among these requirements, the permeate (or product) flux and the rejection are the most important performance metrics. If the flux of the membrane is higher at a given driving force, the area required for a membrane for a given permeate flow rate will be smaller; and consequently, the capital costs of the membrane will be lower. As well, membranes with higher selectivity are more desirable since less processing will be required to achieve a product of a given purity.

Normally, membranes with high porosity and narrow pore size distribution are used in dialysis, ultrafiltration, and microfiltration applications (Pinnau & Freeman,

2000). On the other hand, in reverse osmosis, pervaporation, and gas separation membranes with a dense selective layer are used. Also, Villaluenga et al. (2005) have claimed that according to the solution/diffusion mechanism, flux is inversely proportional to the membrane thickness; therefore, the selective layer in ideal dense membranes should be very thin. Even a few defects in a membrane can produce a remarkable decrease in selectivity, thus, the formation of a molecularly dense thin separating layer is desired.

Ulbricht (2006) has claimed that although tailor-made polymers have been developed with an excellent selectivity and permeability, only a few of them were utilized in commercial applications. The process of applying new membrane materials has been very slow due to other important performance requirements. For instance, mechanical strength, chemical resistance, and thermal stability should be considered in the assessment of new membrane materials (Le & Nunes, 2016). Under industrial operating conditions, it is critical that membranes show stable long-term separation characteristics. Over time many of these membranes experience a decrease in separation flux or selectivity, and basically they need to be replaced regularly. Long-term use of current membrane types is limited by fouling, swelling, and even chemical destruction.

2.1.1 Membrane types and formation method

Membranes can be classified by their geometry, bulk structure, separation regime, manufacturing method, and operation; as is shown in Figure 2.1. There are two main types of membrane geometries: flat sheet or tubular (hollow-fiber). Flat sheet membranes are packed in plate-and-frame systems or spiral-wound modules, while tubular membranes are packed in hollow- fiber modules. Although hollow-fiber modules have better membrane area per module volume, spiral-wound modules are frequently utilized in large-scale separation processes. Bulk structure of membranes can be symmetric (isotropic) or asymmetric (anisotropic).

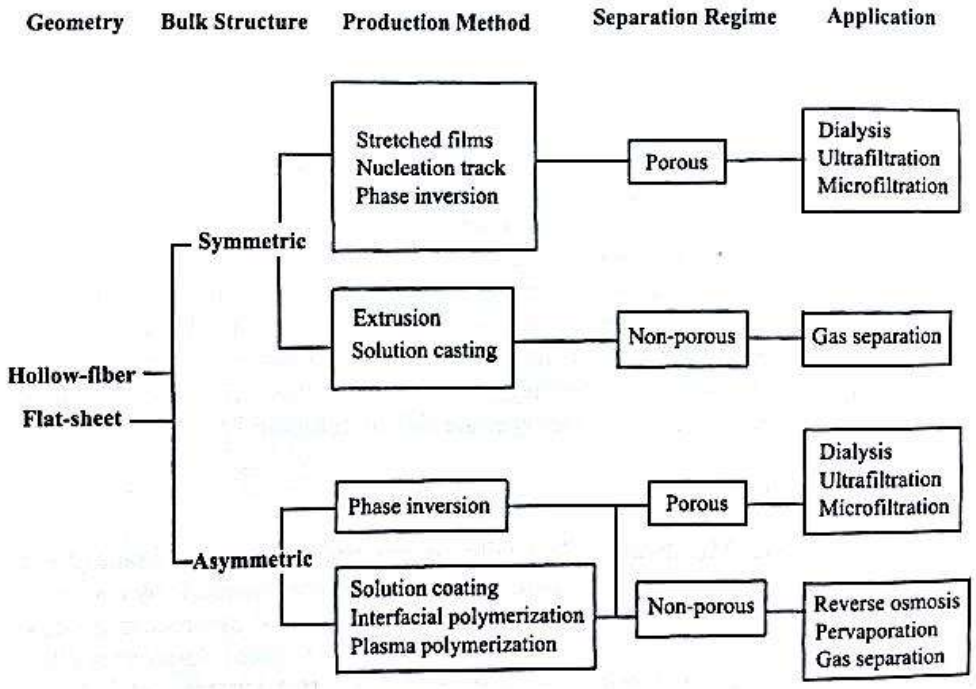

Figure 2.1 Synthetic membrane classification based on their geometry, bulk structure, separation regime, manufacturing method, and operation (Pinnau & Freeman, 2000)

Symmetric membranes have a uniform cross-section (Figure 2.2). On the other hand, the structure of asymmetric membranes changes from its skin or top surface to its base.

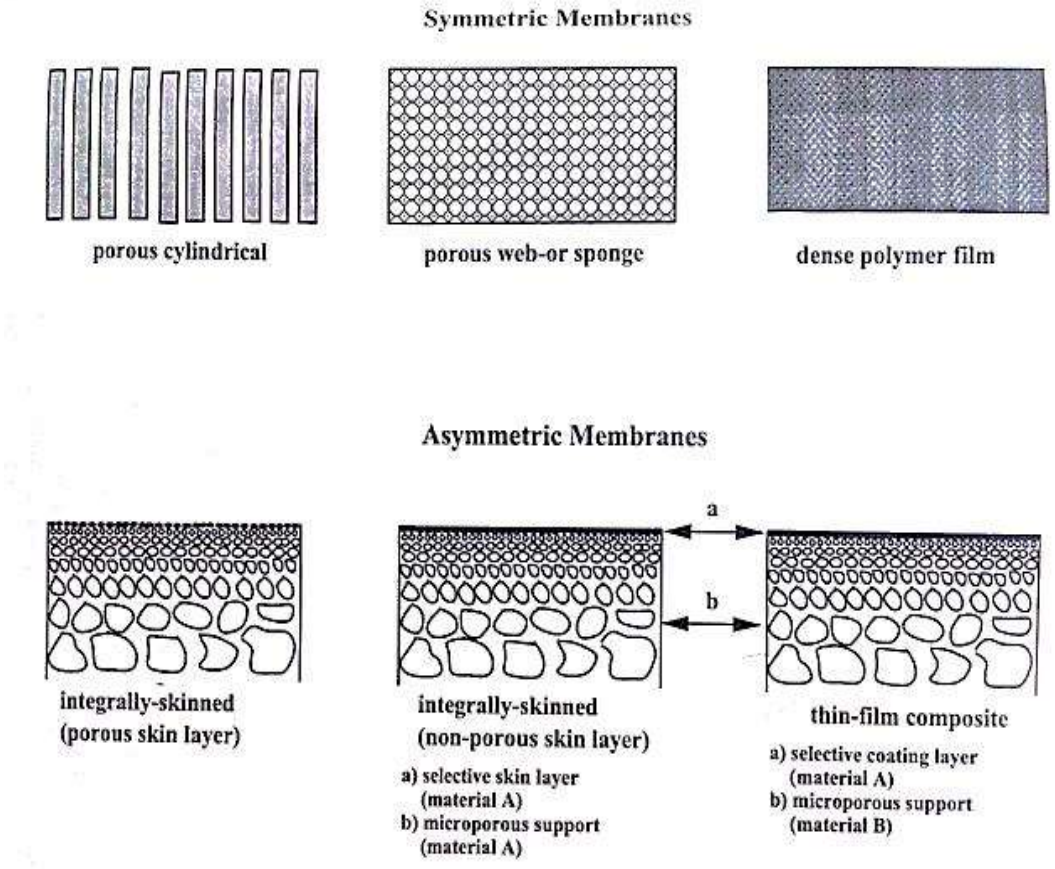

Figure 2.2 Representational of the cross-section of symmetric and asymmetric membranes (Pinnau & Freeman, 2000)

2.1.2 Symmetric membranes

Khulbe (2008) has claimed that the pores of symmetric membranes are cylindrical, sponge like, web-like or slit-like, and various techniques are applied to produce them. He added that irradiation, stretching of a melt-processed semi-crystalline polymer film, temperature-induced phase separation, and vapour-induced phase separation, are the most important production methods of porous symmetric membranes. Irradiation-etching process is used to produce cylindrical porous structure in symmetric membranes. This process has two steps; first, charged particles irradiate dense polymer film. Then, in the second step the film is contacted with a sodium hydroxide solution as an etchant medium. During the first step, charged particles irritate a dense polymer film, such as polycarbonate, which leads to nucleation tracks across the cross-section. In second step (etching) pores are formed due to the partial degradation of the polymeric film in the nucleation track. Buonomenna et al. (2011) believe that pores produced by this method are uniform in size, and the irradiation and etching times can control the porosity and the pore size of the membrane.

Moreover, Pinnau and Freeman (2000) explained that polyethylene and polypropylene, as semi-crystalline polymers, are used for making membranes that have symmetric slit-like porous structure by the melt extrusion/stretching method. First, a semi-crystalline polymer is melted and extruded to form a row of nucleated lamellar structures and under high stress re-crystallization occurs. Then, the membrane is stretched in a machine to form slit-like pores between the stacked lamellae along the direction the membrane is being pulled.

For the sponge-like or web-like pores, the vapour-precipitation process is applied. In this method, a solution of polymer, solvent, and non-solvent is cast on a suitable substrate and then, is exposed to an air stream that is saturated with water-vapour. Due to the water vapour, phase separation occurs in the initially uniform polymer solution. Then, a hot air stream is blown across the membrane so that, the solvent and non-solvent evaporate. Figure 2.3 shows the cross section of the membrane made by precipitation/evaporation process. The polymer concentration and humidity are important in controlling the porosity and the pore size of the resulting membrane. Pinnau and Freeman (2000) declared that high porosity membranes with large pores are produced when the polymer concentration is low and the relative humidity is high. They also added that adding solvent vapour to the casting atmosphere can also create large pores.

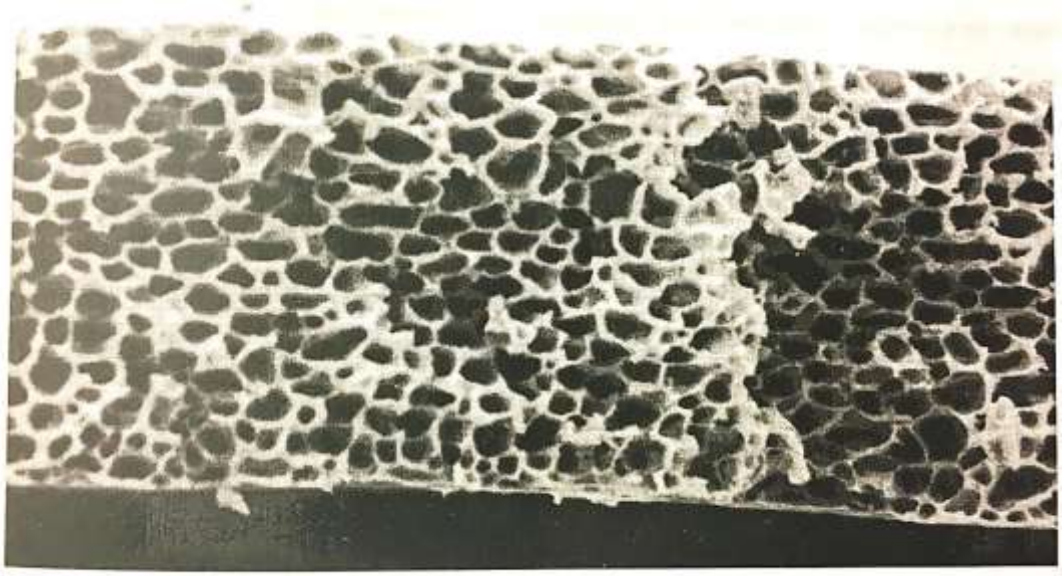

Figure 2.3 Cross section of polysulfone symmetric membrane that is produced by vapour- precipitation/evaporation method (Pinnau & Freeman, 2000)

2.1.3 Asymmetric membranes

As described by Ladewig and Al-Shaeli (2017) based on their structure there are three kinds of asymmetric membranes: 1) integrally asymmetric- membranes with a porous skin layer; 2) integrally asymmetric membranes with a dense skin layer; and 3) thin- film composite membranes. Integrally asymmetric membranes with a porous skin layer are utilized in dialysis, ultrafiltration, and microfiltration, while integrally asymmetric membranes with a dense skin layers are used in reverse osmosis and gas separation (Ladewig & Al-Shaeli, 2017). They also reported that thin-film composite membranes have a thin selective layer on top of a porous support layer, and the materials for each layer can be chosen independently; essentially, this type of membrane is produced for reverse osmosis although currently they are primarily utilized in nanofiltration, gas separation, and pervaporation applications.

The Immersion precipitation process is used to produce integrally-skinned asymmetric membranes from a binary solution which contains a polymer and a solvent. The cast solution is spread over a surface to form a film, and then the solution- film is immersed into a liquid (the non-solvent) and mixed. Then, some of the solvent diffuses into the non-solvent but the polymer does not; this results in a porous or non-porous skin layer of asymmetric structure formation. In integrally–skinned asymmetric membranes there is a structural gradient as a result of precipitous polymer concentration in the developing membrane at the beginning of the phase separation (Buonomenna et al., 2011). Phase separation in immersion precipitation is generated via solvent evaporation or solvent/non-solvent exchange during quenching.

Polymer, solvent, and non-solvent (plus possibly additives) are the main components that are used in immersion precipitation processes to produce commercial membranes. Even addition of a very small amount of non-solvents to the casting solution (alcohols, carboxylic acids, surfactants, etc.), inorganic salts ($LiNO_3$ or LiCl), or polymers (polyvinylpyrrolidone, polyethylene glycol) can modify the porosity, pores size, and thickness of the skin layer. Table 2.2 illustrates examples of components that are used in the immersion precipitation process to produce membranes.

Table 2.2 Common multi-components used for producing membranes by immersion precipitation (Pinneau & Freeman, 2000)

Polymer	Solvent	Non- Solvent Or additive	Quench medium	Application
22.2 wt% CA	66.7 wt% acetone	10.0 wt% Water+1.1 Wt% $MgClO_4$	water	RO
16.2 wt% PSF	79 wt% DMAc	4.8 wt% PVP	70.5 wt% IPA+29.5 wt% water	UF
10.46 wt% PES	69.72 wt% DMF	19.82 wt% t-amyl alcohol	water	MF
37 wt% PSF	36 wt% NMP	27 wt% Propionic acid	water	GS
18 wt% PI	82 wt% p-chlorophenol	-	35 wt% water + 65 wt% ethanol	GS

CA= cellulose acetate; PSF=polysulfone; PES=polyethersulfone; PI=polyimide; PVP=polyvinylpyrrolidone; DMAc=dimethylacetamide; DMF=dimethylformamide; NMP=N-methylpyrrolidone

According to Pinnau and Freeman, (2000), the specific parameters that affect formation of membranes in immersion precipitation method are:

- Characteristics of the polymer (molecular weight, molecular weight distribution)
- Characteristics of the solvent
- Characteristics of the additives
- Proportion of the base polymer, solvent and additives in the casting solution
- Temperature of the casting solution
- Characteristics and temperature of the quench medium
- Composition and temperature of the atmosphere
- Evaporation conditions
- Cast film thickness
- Casting speed
- Material of membrane support (type of woven or non- woven)
- Drying conditions

2.1.4 Thin-film composite membranes

Thin-film composite membranes are composed of at least two layers that are made of different materials (Ladewig & Al-Shaeli, 2017). They can consist of a single thin selective layer and a porous sublayer, or multi layers with different functions. In single thin–layer membranes, the first type, mechanical strength is provided by the porous support while the top-layer governs the separation. In the multi-layer membranes, the second type, each layer has a specific function.

Thin film composite membranes have several advantages over the integrally-skinned asymmetric membranes such as: 1) different materials can be chosen and different preparation methods can be applied for the separating layer and the porous sublayer; 2) Only a very small amount of polymer is used for the selective layer, therefore, very expensive membrane materials can be used (Naylor, 1996).

Low et al. (2015) claimed that in many cases, mechanical support for the thin-film composite membranes is provided by an ultrafiltration membrane that is produced by the immersion precipitation method and is porous. The porous support layer should be chemically resistant to the solvent or solvent mixture used for the formation of the selective layer. Also, it should have small pores and high surface porosity.

Lau & Ismail (2011) claimed that solution coating and interfacial polymerization methods are the most important techniques to produce commercial thin-film composite membranes. In the solution coating technique, the surface of a porous support, such as substrate or backing material, is covered by direct deposition of a diluted polymer solution. Regardless of the shape (flat sheet or hollow fibre support) before coating, the

porous support is immersed into a bath of dilute polymer. Then, the membrane is taken out of the bath and the solvent evaporates and a thin layer of polymer forms on the surface of substrate membrane. The thickness of this coating layer is usually less than 2 μm and contains defects. Also, the coating polymer solution may penetrate into the pores of the substrate membrane (Khayet & Matsuura, 2011).

In interfacial polymerization or in-situ technique, a nonporous top layer is created on a porous substrate via a polymerization reaction; this occurs when two reactive monomers react at the interface of the two un-mixable solvents. The porous substrate is saturated by an aqueous solution which contains a reactant, such as a polymeric amine, and then the porous substrate is immersed, an un-mixable organic solvent (such as hexane), that contains a reagent like di- isocyanate. As a result of the reaction of the two monomers at the water-organic solvent interface, a dense layer forms on top of the porous substrate (Baker, 2012).

2.2 Membrane processes

Microfiltration (MF), ultrafiltration (UF), nanofiltration (NF), and reverse osmosis (RO) are four types of pressure-driven membrane processes that are applied currently in municipal water treatment (MWH, 2012). Types of materials rejected, operating pressures, and nominal pore dimensions can relatively identify membranes. Figure 2.4 shows the hierarchy of membrane processes.

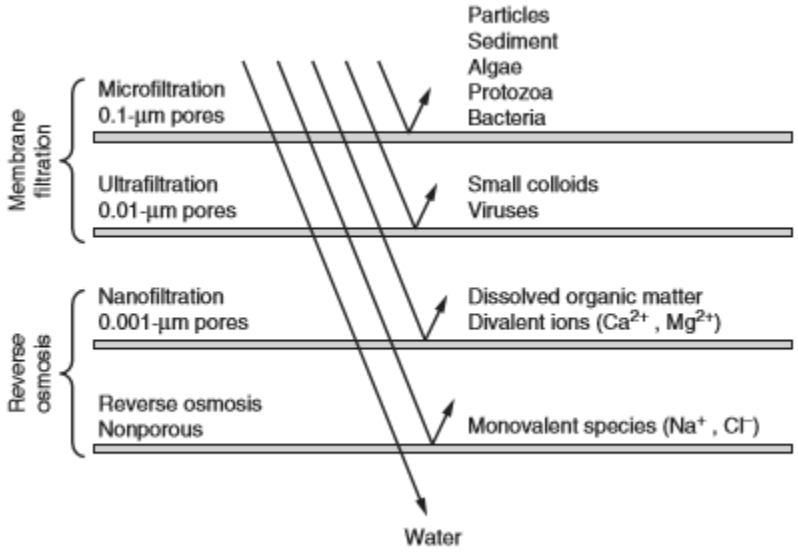

Figure 2.4 Separation capabilities of pressure-driven membrane processes used in water treatment (MWH, 2012)

2.2.1 Ultrafiltration:

Ultrafiltration (UF) membranes have pore sizes of approximately 0.002 to 0.1 microns, molecular weight cut-off from 10000 to 100000 Daltons, and the required operating pressures ranging from 206 to 689 kpa [30 to 100 psig]. UF membranes are extensively used in the production of drinking water from freshwater sources. Ultrafiltration will remove all types of protozoa and bacteria, some viruses and some humic materials.

However, since UF membranes are not absolute barrier for all viruses, in drinking water treatment post-membrane chemical disinfection is recommended as a second barrier to viruses. Ultrafiltration has a wide application in many industrial processes with high separation efficiency such as water purification, biological filtration, and beverage clarification (Dobosz et al., 2017). To improve the performance of UF membranes it is necessary to simultaneously improve the permeability and selectivity by controlling their structure (Fang et al., 2015). Fang et al. (2015) also declared that high membrane permeability is achieved by membranes with thinner skin layers and larger pore density; while better selectivity occurs by thinner skin layer and smaller pore sizes. Usually, the material for ultrafiltration membrane is either organic or inorganic (Chen et al., 2013) and the most common polymeric ultrafiltration membrane preparation method is the phase inversion process (Fang et al., 2015). Compared to conventional clarification and disinfection processes, the principal advantages of low-pressure ultrafiltration membranes are (Foley, 2011):

- Less chemicals such as coagulants, flocculants, disinfectants, and pH adjustment are required
- Size- exclusion filtration in contrast with media depth filtration
- Constant quality of the purified water regardless of fluctuations in the feed water quality
- Compact units resulting in smaller treatment plants
- Uncomplicated automation

2.3 Membrane fouling

Zhao et al (2000) claimed that most membrane separation processes save energy and do not require phase change; therefore, they are widely used technologies and are a better substitution for some of the conventional separation processes. Compared to distillation and evaporation processes, membrane separation are non-thermal methods and have higher efficiency. Thus, industries such as the pharmaceutical and the food industry apply membranes for many separation processes. Although there is a great interest in membrane technology and its applications, their efficiency is affected by fouling and concentration polarisation (Zhao et al., 2000).

Accumulation of solutes in the pores or on the surface of the membrane causes fouling which reduces membrane permeability (Duranceau, 2001). Also, membrane rejection is affected by fouling. There are two types of fouling: reversible, which can be removed by hydrodynamic or chemical cleaning processes, and irreversible which cannot. Only the flux loss caused by reversible fouling can be recovered (Duranceau, 2001).

Shi et al. (2014) declared that concentration polarisation is a specific problem throughout filtration process of low molecular weight solutes or macromolecules. During filtration, the permeation flow carries solutes towards the membrane surface, where larger solutes are rejected by the surface of the membrane while the solvent molecules pass through the membrane. Thus, the rejected molecules accumulate near the membrane surface and diffuse back to the bulk solution very slowly, which leads to a concentration gradient above the surface of the membrane. The concentration of the rejected molecules near the membrane surface becomes sometimes 20-50 times of the bulk solution (Shi et al., 2014). The accumulated molecules delay the flow of the solvent through the

membrane and causes osmotic back pressure which reduces the effective transmembrane pressure (TMP) of the system. Although concentration polarisation is an unavoidable phenomenon, it does not have impact on innate properties of a membrane. If the feed is switched to the pure-solvent stream, the flux loss will be recovered. Accumulation of solutes at the upstream surface of a membrane leads to concentration polarization, which is considered as a hydrodynamic/diffusion phenomenon (Zhao et.al, 2000). Operating the system at higher velocity may facilitate reduction of this phenomenon. Usually, concentration polarization occurs in any membrane processing due to fundamental restrictions of mass transfer and actuality of a boundary layer.

In addition, deposition of matter on the surface of a membrane or inside its pores causes membrane fouling. Irreversible loss of membrane permeability may occur by fouling in contrast to reversible flux decline caused by concentration polarisation.

2.3.1 Types of fouling

Adsorption, pore blocking, and cake or gel formation are the mechanisms that cause fouling in ultrafiltration. Adsorption occurs due to specific interactions between particles or solutes in the solution and the membrane. Depending on which functional group is involved, interactions are weak Van der Waals, electrostatic interactions, or chemical bonds (Shi et al., 2014). In addition, formation of a monolayer of solutes on the surface of the membrane can occur instantaneously and spontaneously even in the absence of permeate flux. This phenomenon may become irreversible as it happens in the separation of some humic acids (HA) and proteins; humic acids are diverse in composition, many are hydrophobic in nature, so, they have a strong affinity for the membrane surface (Shi et al., 2014). Only chemical cleaning is effective for membranes

fouled with these macromolecules. The hydrophobicity of the membrane material may make it more prone to fouling particularly by hydrophobic solutes. Hydrophobicity and charge characteristics of the membrane are affected by the adsorbed materials (Shi et al., 2014).

Pore blocking, cake, and gel formation are considered as internal and external fouling, respectively. When colloids and particles block the pores fully or partially, pore blockage forms and it usually occurs rapidly in the initial phases of filtration before the cake and gel formation.

As Shi et al., (2014) have described, cake layer forms when particles precipitate layer by layer on the membrane surface causing an extra resistance to the permeate flow. Both chemically inert and active colloids can form the cake layer. The first layer of inert colloids near the surface of the membrane prevents active colloids from contacting the membrane surface. This is called a “filter aid”. In contrast, it may happen that the first layer is formed by the active colloids that will act as a bridge for inert colloids; this phenomenon creates a more adhesive cake and more irreversible fouling. When small macromolecules enter and penetrate the openings within the cake, “over clogging” occurs and this leads to a considerable hydraulic resistance. While Shi et al. (2014) declared that the interaction between the membrane surface and cake layer determines the fouling reversibility, morphology of the cake layer controls the flux decline.

Gel formation occurs when the concentrated layer of macromolecules is formed in the vicinity of the membrane surface due to concentration polarisation. Concentration polarization transits to fouling when the attractive electrostatic force becomes greater than the repulsive force. Shi et al. (2014) claimed that at a certain flux gelation occurs and this flux is marked as limiting flux that represents the maximum stationary permeation flux reached through increasing trans-membrane pressure (TMP). In general, mechanism of fouling depends on operating conditions, feed streams, and membrane properties.

2.3.2 Foulants

Shi et al. 2014 claimed that particulates, macro-molecules, ions, and biological matter are four main types of substances that often cause problems in ultrafiltration processes, as summarized in Table 2.3.

Table 2.3 Foulants and their modes of fouling (Shi et al. 2014)

Examples of foulants and their fouling modes in major membrane applications involving liquid–solid separation.

Foulants	Fouling modes
Large suspended particles	Particles present in the original feed or developed due to aggregation can form a cake layer and/or block module channels
Small colloidal particles	Colloids present in recovery of cells from fermentation broth can form a dense cake layer. They can also block the entrance of a membrane pore or clog inside of it
Inert macromolecules	Gel or cake formation on membrane
Adsorptive macromolecules	Proteins and HAs are known to adsorb on to surfaces on membranes or in the pores
Small molecules	Some small organic molecules tend to have strong interactions with some polymeric membranes (e.g., anti-foaming agents, such as polypropylene glycols used during fermentation, adhere strongly to certain polymeric membranes)
Biological substances	The growth of biologically active organisms such as bacteria and their excreted material aka EPS form biofilms on membrane surfaces
Cations	Precipitation of salts and hydroxides to form scaling. Certain cations such as calcium can facilitate macro-molecular foulings

Size of particulates varies from 1 nm to 1 μm with a rigid shape (Belfort, Davis, & Zydney, 1994). Depending on the ratio of the particle size and the membrane pore diameters, the pores can be blocked completely or partially, which reduces the effective pore size. Over the length of filtration, a certain cake layer forms after pores have been blocked. Inter-particle interactions and therefore, the properties of the fouling cake are determined by colloidal characteristics such as surface charge, roughness, size, hydrophobicity and stability (Shi et al., 2014). Foulants may have molecular weight from 1 million to a few thousand Daltons or smaller. Other than fouling by particles the main types of foulants are natural organic matter, inorganic scaling, and biofouling.

2.3.2.1 Natural organic matter

Natural organic matter (NOM) was classified by Shi et al. (2014) according to the NOM's origin and source: i) allochthonous organic matter originates from floral debris and terrestrial sources, ii) autochthonous organic matter consisting of extracellular, intercellular, and cellular debris from natural aquatic sources, iii) NOM from wastewater effluents (EfoM) that contains background NOM and soluble microbial products (SMPS) generated by biological wastewater treatment plants. According to Shi et al. (2014) NOM has a complex chemistry due to the wide range in size of the heterogeneous mixture of macromolecules, functional groups, and sub structures. They also declared that the majority of these macromolecules in natural waters are humic substances; they represent approximately 80% of the total organic carbon in the water. Based on the solubility of humic substances in acidic solutions, NOM is categorized into three fractions: 1) insoluble humin; 2) humic acids (HA) which are insoluble at pH<2; and 3) fulvic acids (FA) which are soluble at any pH. Polysaccharides, carbohydrates, amino acids, and proteins are the other fraction (20%) of NOM.

In NOM filtration the feed is complex and it is generally difficult to identify an individual fouling mechanism; the effects are combined. For example, HAs provide a bridge between membrane polymers and alginate gels, which causes a more irreversible fouling layer (Jermann et al., 2007). Compressing the electrostatic double layer and smoothing colloidal aggregation are caused by HAs, which may lead to changing the state of colloidal particles (Tombacz et al., 2004; Tombacz & Szekeres, 2006; Contreras et al., 2009).

2.3.2.2 Scaling

Scaling from metal ions can be a significant problem of UF under specific circumstances. Iron salts are sometimes used as a coagulant agent in membrane pre-treatment of surface waters with medium to high turbidities and NOM concentrations. The Fe salts form $Fe(OH)_3$ flocs that can form a sticky brown fouling layer on the membrane surface. Shi et al. (2014) declared that the magnitude of the fouling caused by cation flocs can be greater than that by the foulants themselves. Divalent cations provide a bridge between NOM molecules that have a net negative charge. Also, Shi et al. (2014) claimed that although the membrane surface is negatively charged the presence of monovalent cations increases the ionic strength and weakens electrostatic repulsion force.

2.3.2.3 Membrane biofouling

Shi et al. (2014) have provided that membrane biofouling is caused by active microorganisms when they adhere to the membrane and form a biofilm by growing. The process begins by adsorption of existing macromolecules in the feed such as proteins, polysaccharides, HAs, and extracellular polymeric substances (ESP) discharged from the microorganisms, and formation of a conditioning film on the membrane surface. They form a gel-like film that causes an immediate extra resistance to the permeate flow. An uneven deposition forms due to attachment of micro-organisms onto the membrane surface. Nutrients and organics from the feed are brought to the membrane surface by convective flows and concentration gradients (diffusion). Shi et al. (2014) claimed that the colonisers grow on these transferred nutrients and organic and eventually, form a joining and mingling biofilms. These biofilms may be heterogeneous, dwelling different species of micro-organisms, and stratified, containing a layer with an aerobic population

at the top and another layer consisting anaerobic population underneath, this is provided by Schaefer et al. (2005). As Le-Clech et al. (2006) have discussed, these biofilms are a major issue in MBRs (membrane bio reactors) and RO systems.

2.4 Factors affecting membrane fouling

2.4.1 Impact of feed properties

2.4.1.1 Concentration

According to Olson (1977) and Balmann et al. (1989), increasing the feed concentration leads to a decline in permeate flux but does not have remarkable effect on the membrane retention characteristics, unless the size of components change with concentration. As well, increasing concentration has little impact on irreversible membrane fouling but reversible cake and gel formation is increased. Furthermore, increasing concentration increases the rate of membrane fouling when internal membrane fouling is dominant. However, cake or surface fouling is presumed to dominate at high concentration feeds.

2.4.1.2 pH and ionic strength

Proteins are complex molecules and their interactions with the membrane surface are affected by pH and ionic strength, therefore, protein fouling is not clearly understood. There are three explanations for the effects of ionic strength and pH on membrane-protein interactions: 1) the change in protein configuration and stability affects the tendency of the protein to deposit on the membrane; 2) the change in the protein effective size affects the porosity of the dynamic membrane; and 3) the change in charge difference between the membrane surface and protein affects protein deposition or adsorption (Zhao et al., 2000).

2.4.1.3 Constitution interactions

When there are large and smalle molecules that coexist in the feed solution, the larger molecules may be adsorbed first due to their stronger interaction with the membrane, leading to the partial pore blocking. Then the smaller molecules are rejected by the smaller pores formed between the larger molecules (Zhao et al., 2000).

2.4.1.4 Prefiltration and aggregates removal

When proteins agglomerate, larger membrane pores are blocked, causing disproportionate loss of flux and the formation of a protein foulant layer on the membrane surface (Zhao et al., 2000). Permeate flux in UF and MF can be improved by prefiltration in which large molecular weight compounds are removed (Tanny et al., 1982).

2.4.2 Effect of membrane physio-chemical characteristics on membrane performance and fouling

In general, membrane fouling is influenced by: a) the morphology of the membrane surface; e.g. surface roughness, pore size, and porosity, and b) the physio-chemical characteristics of the membrane.

2.4.2.1 Pore size

Numerous studies have shown that increasing the pore size leads to more severe membrane fouling (Gatenholm et al., 1988; Balmann et al., 1989). There is an optimum pore size; below the optimum size the permeate flow is restricted due to the resistance of the membrane and above the optimum size the flux decreases due to the serious membrane fouling.

2.4.2.2 Porosity and pore size distribution

Zhao et al. (2000) have claimed that the majority of UF and MF membranes possess a broad pore size distribution. The total permeate flux is controlled by the flow through the largest pores, therefore, fouling or plugging of the large pores such as by protein aggregation, affect the permeate flux. Membranes with a wide pore size distribution have poor selectivity. Pore size distribution and pore density are changed by membrane fouling. Thus, as the membrane gets fouled over the time, membrane selectivity, component retentions, and permeate flow are changed (Zhao et al., 2000).

2.4.2.3 Physico-chemical properties

Zhao et al. (2000) explained that physio-chemical interactions between solutes and membrane materials may change under different circumstances. The two main physio-chemical interactions are charge and hydrophobic effects. They added that the membrane material, the pH, and ionic strength of the feed determine the charges on the membrane. Electrostatic interactions between the solute and the membrane are either attractive or repulsive. Both solute and membrane charges are effected by the pH of the feed solution. As well, as the ionic strength of the feed solution increases, the thickness of the double layer is reduced, this weakens the electrostatic interaction.

Nakao et al. (1988) showed for membranes that had a similar charge to the protein charge, the permeate flux may be higher if the concentration polarization is less. They explained that this occurs by repulsion of same electrostatic charges between membrane and proteins, and it results in a smaller concentration polarization layer and ultimately, lower flux reduction.

According to Fane and Fell (1987) hydrophilic membranes adsorb less protein and potentially have higher permeate fluxes than hydrophobic membranes. However, when multilayers of adsorbed proteins form due to high concentration polarization and protein deposition, the effect of membrane surface hydrophilicity/phobicity is hidden.

2.4.3 The effect of the membrane operating factors

The permeate flux and fouling are impacted by a number of factors in membrane operating system. These factors include the transmembrane pressure, temperature, and cross-flow velocity and turbulence.

2.4.3.1 Transmembrane pressure

Zhao et al. (2000) showed that in low pressure filtration (TMP< 4 bar), increasing the transmembrane pressure leads to an increase in permeate flux and an increase in the fouling rate. Increasing concentration polarization can decrease the membrane rejection. However, in the long term the retention of component by UF membranes increases because the rate of fouling is increased (Zhao et al., 2000).

2.4.3.2 Temperature

Zhao et al. (2000) declared that increasing temperature results in an increase in the permeate flux due to the decrease in the liquid viscosity. Edzwald (2010), in his water quality and treatment handbook, also claimed that increasing temperature also increases the solute diffusivity and permeate flux, and thus reduces the concentration polarisation effect.

2.4.3.3 Cross-flow velocity and turbulence

Zhao et al. (2000) claimed that permeate flux improves in UF and MF by increasing the cross-flow velocity due to a reduction in the gel layer formation. They added that increasing velocity decreases membrane fouling and increases effective pore size. They explained that the cross-flow velocity does not have any effect on the irreversible fouling as it is primarily due to fouling in the membrane pores. In addition, they claimed that generating higher turbulence at the membrane surface causes an enhancement in mass transfer and a greater membrane flux.

2.5 Membrane cleaning

Membrane cleaning methods are categorized into four types: Physical, chemical, physio-chemical, and biological techniques.

2.5.1 Physical cleaning methods

According to Pearce (2011) in physical membrane cleaning methods the foulants are removed mechanically from the membrane surface. These methods include periodical backflushing of hollow fiber membranes, cross-flow flushing of flat sheets and spiral wound membranes, vibration, air sparging, and ultrasonication. The optimization of ultrasonic cleaning procedures for ultrafiltration membranes in the dairy industry was attempted by Muthukumaran et al. (2004).

2.5.2 Chemical cleaning methods

Zhao et al. (2000) have provided that this technique is dependent on chemical reactions that remove foulants from the membrane surface. Normal functional capacity and separation properties of the membrane should be restored while deposits are removed by the chemical cleaning process. They added that chemicals should dissolve the foulant at the membrane surface, but should not destroy the membrane or other parts of the system. Examples of cleaning agents include: alkalis (hydroxides, carbonates); acids (nitric and phosphoric); surface- active agents (anionic, cationic, and non-ionic); and sequestering agents: (EDTA) (Zhao et al., 2000). Chlorine solutions are often used to clean NOM fouled membranes.

2.5.3 Physico-chemical cleaning methods

Physical and chemical cleanings are combined in order to enhance cleaning efficiency. Zhao et al. (2000) mentioned that a physio-chemical cleaning method has been performed by Kuiper and his colleagues to clean cellulose acetate RO membranes fouled by a highly polluted source for 19 months. The most effective cleaning method was mechanical cleaning (such as depressurising and flushing with the foam balls) enhanced by acid washing.

2.5.4 Biological cleaning methods

Foulants are removed by cleaning mixtures that contain bioactive agents. Enzymes are the most effective cleaning agents for this purpose (Zhao et al., 2000).

2.6 Approaches for improving membrane performance

Methods to avoid reduction of membrane performance due to membrane fouling and concentration polarization are classified in four categories: control of boundary layer, turbulence generator or persuader, membrane materials, and membrane modification.

2.6.1 Boundary layer or velocity control

Al-Bastaki and Abbas (2001) have claimed that thickness of the boundary layer adjacent to the membrane can be reduced by increasing the cross-flow velocity of the feed solution. They also mentioned that flow pulsation causes the boundary layer thickness to oscillate and helps prevent the formation of gel layers. They explained that the flow pulsation is used in addition to a periodic backwashing from the permeate side in order to minimize concentration polarization.

2.6.2 Turbulence generator

Turbulence generators and persuaders include ribbed spacers and channels, additional particles or spheres with different densities, and ribbed or wavy membranes (Zhao et al. 2000). The increased turbulence they create help reduce the thickness of the boundary layer and thus reduce the extent of concentration polarization.

2.6.3 Membrane material and modification

Contact of foulants with the membrane can be minimized by velocity and turbulence on the surface of the membrane. Nevertheless, eventually, foulants will interact or react with the membrane. Thus, membrane fouling can be reduced by minimizing these interactions. The development of new membrane materials and the modification of membrane surfaces are helpful for reducing membrane fouling (Zhao et al., 2000).

Hydrophilic and homogeneously permeable membranes are ideal UF membranes for the majority of applications. To this end, membranes are often pretreated by surfactants or by hydrophilic polymers such as: methylcellulose (MC), polyvinylalcohol (PVA), and PVP, especially when the foulant is a protein (Zhao et al., 2000). Initial UF flux increases and flux decline decreases via this treatment.

Surface Thin-film (–layer) (TFL) coating is a technique to modify the membrane surface (Matsuura & Rana, 2010). They added that TFLs can be coated via non covalent or Van der Waals bonding by using materials that are hydrophilic or negatively charged.

In addition, they explained that surface- modifying macromolecules (SMM) are polymers or macromolecules blended in the membrane casting solutions and during the

casting these macromolecules tends to migrate toward the surface of the membrane in order to decrease the surface energy, as confirmed by Zhang et al. (2003). Matsuura & Rana (2010) explained that by controlling the amount of mitigated components the membrane surface can be modified by blending even small quantity of macromolecules. This is a one step process and does not require an extra surface-modification step (Nguyen et al., 2007; Pezeshk, et al., 2012).

2.7 Electrospinning

Nasreen et al. (2013) have claimed that one of the recent developments in membrane fabrication and modification is the application of nanotechnologies. Various materials such as polymers and inorganic metal/polymer composite can be used in their nano-scale structures. They also added that among others, electrospun nanofiber membranes (ENMs) have attracted much attention recently due to their high porosity of interconnected pores, the high surface to volume ratio, simplicity of electrospinning.

Electrospinning is a flexible method for producing nanofibers with various diameters and different morphologies (Nasreen et al., 2013). It is capable to produce nanofibers of nanometer to micrometer size. The formation of nanofibers is governed by several electrospinning conditions such as: the electrospinning solution flow rate, the applied voltage, the electrospinning chamber humidity, and the distance between the tip of the extrusion needle and the nanofiber collector. Figure 2.5 presents a schematic an electrospinning set-up.

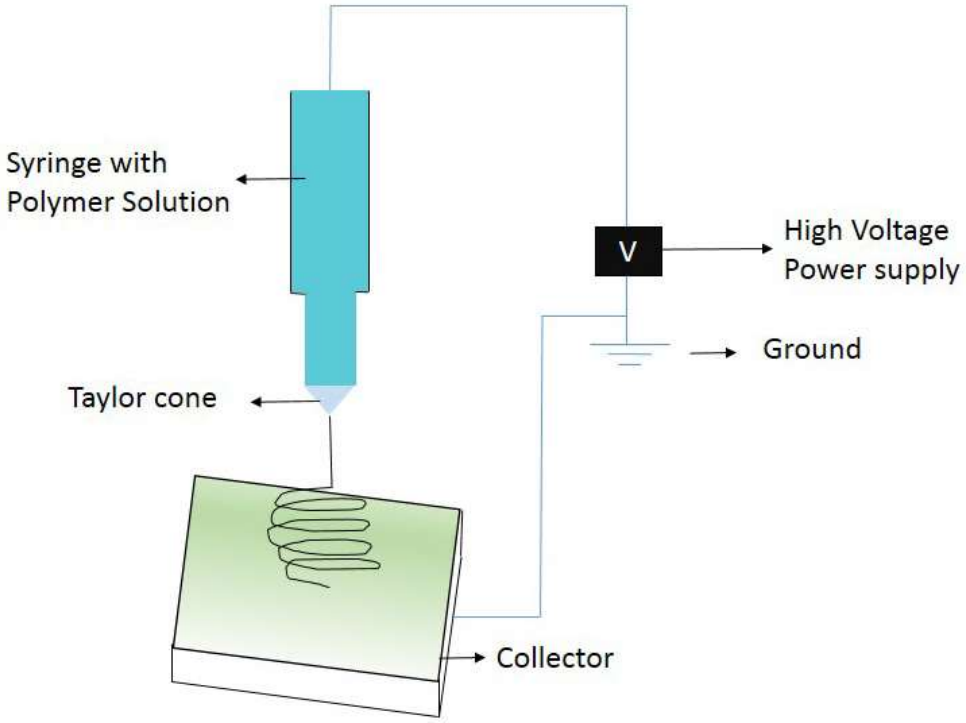

Figure 2. 5 Electrospinning system (Nasreen et al., 2013)

Nasreen et al. (2013) explained that in this process, a jet of polymer solution, which is electrically charged, is extruded from a syringe; this occurs due to the application of a high voltage to the syringe needle. The voltage is applied gradually until it overcomes the surface tension of the polymer solution and a Taylor cone (of the polymer solution) materializes out of the needle and rotates down as a fiber towards a collector plate. Prior to reaching the collector plate, the solvent in the polymer solution evaporates and the polymer hardens and is collected as fibers. The voltage power supply is connected to a syringe needle from one side and from the other side to a grounded collector. Surface tension holds the solution from the jet and will be overcome once it produces a charge on the surface of the liquid. Repulsion and contraction of the surface

charges to the counter electrode generate an opposite force directly to the surface tension. By increasing the voltage, the Taylor cone initiated from the tip of needle surface lengthens. The discharged polymer solution jet experiences an instability and elongation process, which permits the jet to create remarkably long, uniform, and thin fibers.

Nasreen et al. (2013) mentioned that electrospinning is a technique with numerous potential applications. However, presently electrospinning is primarily at the research stage involving small membranes; large-scale (commercial) membrane electrospinning has not been fully developed. They also claimed that multijet and needleless electrospinning methods are emerging, which will hopefully permit larger scale membrane electrospinning.

Feng et al. (2013) claimed that more than 100 standard synthetic and natural polymers, such as poly (ethylene terephthalate) (PET), polystyrene (PS), poly (ethylene oxide) (PEO), poly (vinyl chloride) (PVC), poly (vinylidine fluoride) (PVDF), wools, silk, cellulose have been successfully electrospun into nanofibers from their solutions. This occurs due to sufficiently high molecular weight of polymers and the vaporization of solvent during the time of jet transition over the distance between the needle (or spinneret) and the collector (Feng et al., 2013).

There is a problem in handling electrospun nanofibers due to their accumulation of electrostatic charges during the electrospinning process. This happens when the polymer is poorly conductive and the polymer tends to continue, retaining the charges instantly after deposition. Gopal et al. (2006) declared that this problem escalates as the electrospinning thickness increases. Therefore, an additional support different from

conventional membranes is required for facilitating the membrane application and improving the nanofibers strength. Thus, a considerable number of applications of ENMs in membrane separation were built on hybrid systems where nanofibers were "sandwiched" between different layers or combined with micron fibers (Gopal et al., 2006).

Gopal et al. (2006) have declared that in order to alleviate the handling issue of ENM, electrospinning is performed over a more rigid and stronger support. They also mentioned that the strengthening of nanofibers can be conducted by post- heat treatment on the electrospun fibers. They added that nanofibers overlap each other randomly during the electrospinning process, which leads to an open pore structure that is ideal for membranes. They explained that the applied heat should be lower than the melting point (T_m) of constituent material, since otherwise the overlapping fibers would fuse together. This phenomenon, post- heat treatment, improves the structural strength, crystalline structure and mechanical strength of nanofibers and improves nanofiber handling (Gopal et al., 2006).

Once a membrane is created, flux and selectivity are two main factors used to assess membrane performance. Flux describes the rate of transport of permeants across the membrane whereas selectivity is determined by surface properties of the membrane (such as the pore size distribution) that dictates the type of permeant species that can traverse the membrane.

Yoon et al. (2006) have claimed that UF porous membranes that are conventionally manufactured by the phase inversion, inversion precipitation, method and consist of torturous porosity result in a low flux rate. They along with other recent studies (Wang et al., 2012; Khamforoush et al., 2015; Wang et al., 2017, and Dobosz et al., 2017) showed that nanofiber layers provide higher flux and permeability compared to conventional UF membranes.

According to Lee et al. (2014), in water treatment, electrospun nanofibrous membranes are seriously vulnerable to fouling and after some time the fouling deteriorates the permeability and rejection efficiency. They added that many efforts have been made to develop fouling-tolerant membranes by using hydrophilic/hydrophobic interactions or electrostatic repulsions between membrane surface and foulants.

Conventional UF membranes can be used as a support for the electrospun layer in order to enhance the strength of the electrospun layer. Improving the performance of electrospun membranes was also confirmed by Dobosz et al. (2017). Based on the above research there is a need to develop and test alternative electrospun membranes for water treatment. Numerous studies have developed modified membranes mostly using a UF or NF membrane as a support and coated with an electrospun layer of different material; these membranes had higher fluxes than existing commercial membranes. Several of them are described in the Table 2.4.

Table 2. 4 Few studies of electrospun modified membranes and their fluxes

Performed by	**Year**	**Material**		**Type of membrane**	**Flux increase**
		Base	**E-layer**		
Yoon et al.	2006	Scaffold PET[1]	Chitosan[2] & PAN[3]	UF or NF water treatment	magnitude higher flux
Wang et al.	2012	PET	PAN	MF water treatment	2 to 3 times
Khamforoush et al.	2015	PET	PAN coupled with PSF[4]	UF oil/ water	(20 to 160)%
Wang et al.	2017	CS- PLA [5]		oil/water	25 times
Dobosez et al.	2017	PES	Cellulose or PSF	UF water treatment	Permeation by 47% PWP by 35%

[1]Polyethyleneterephthalate; [2]Chitosan:Natural aminopolysaccharides; [3] Polyacrylonitrile; [4] Polysulfone; [5] Chitosan- Poly (lactic acid).

In the studies shown in Table 2.4 various materials were used for both supports and electrospun nanofiber layers to fabricate membranes for different processes such as water and oil filtration. Yoon et al. (2006) used a PET UF/NF membrane substrate with a medium PAN electrospun nanofibrous scaffold coupled and coated with a thin layer of hydrophilic, water resistant, and at the same time water permeable material such as chitosan. Their membrane exhibited an order of magnitude higher flux than the conventional UF or NF porous membranes in water treatment. Wang et al. (2012) used a non-woven PET support coated with the electrospun nanofibers of PAN to show that the flux of the composite MF membrane was 2-3 times higher than the commercial MF membranes of the same pore size (0.22 ± 0.01)μm. Khamforoush et al.(2015) provided a TFC membrane by using non-woven PET support with an electrospun PAN nanofibrous mid layer, and a coating top layer of PSF. The flux of the TFC membrane was 20 to 160% higher than that of the conventional asymmetric PSF membrane. Wang et al. (2017) reported that 25 times higher flux was achieved when CS-PLA nanofiber mats of excellent hydrophobicity and oleophilic properties were collected on number 10 stainless steel mesh wires than collected by number 0 stainless steel wires.

Dobosc et al. (2017) used a commercial PES support on which an electrospun layer of cellulose / PSF blend nanofibers was placed with no adhesion. Only O-rings of the membrane filtration cells held the nanofiber and support layer together to form a composite membrane. The permeation flux in the presence of solute in the feed and pure water permeation flux (PWP) were increased by 47% and 35%, respectively compared to the control membrane.

The above survey thus shows that little attention has been paid so far to coating of electrospun nanofibers on top of the commercial membranes. Accordingly, the aim of this study is to develop a method for modification of commercial and hydrophilic UF membrane coated with a hydrophobic electrospun nanofibers layer, in order to improve the membrane permeation flux. In addition, materials, method of preparation of electrospun modified membrane, and technique of filtration in this study is different from the ones presented in Table 2.4. Therefore, membranes will be developed by coating a commercial PES membrane with electrospun PVDF nanofibers, as PVDF is ideal for drinking water treatment due to its chlorine resistance. Chlorine is sometimes added at the entrance of a water treatment plant and chlorine solutions are frequently used as a chemical cleaning agent.

CHAPTER 3

MATERIALS AND METHODS

This study focuses on potential improvement that can be achieved by modifying the surface of commercial polyethersulfone (PES) membranes by coating them with layers of polyvinylidene difluoride (PVDF) nanofibers produced via electrospinning. This chapter presents the materials utilized in this study, a description of the membrane electrospinning technique, the membrane testing procedures, the analytical methods used and the membrane characterization approaches. The membrane testing consisted of pure water filtration tests of both commercial PES and modified electrospun PES membranes and of fouling tests using solutions of several different proteins as well as Ottawa River water.

3.1 Materials

This study focused on modifying a commercial ultrafiltration membrane. The membrane was a polyethersulfone (PES) membrane produced by Synder Filtration (Vacaville, CA), this membrane has a nominal molecular cut off (MWCO) of 30k. The chemical formula and molecular orientation of PES is illustrated in Fig 3.1 on the following page.

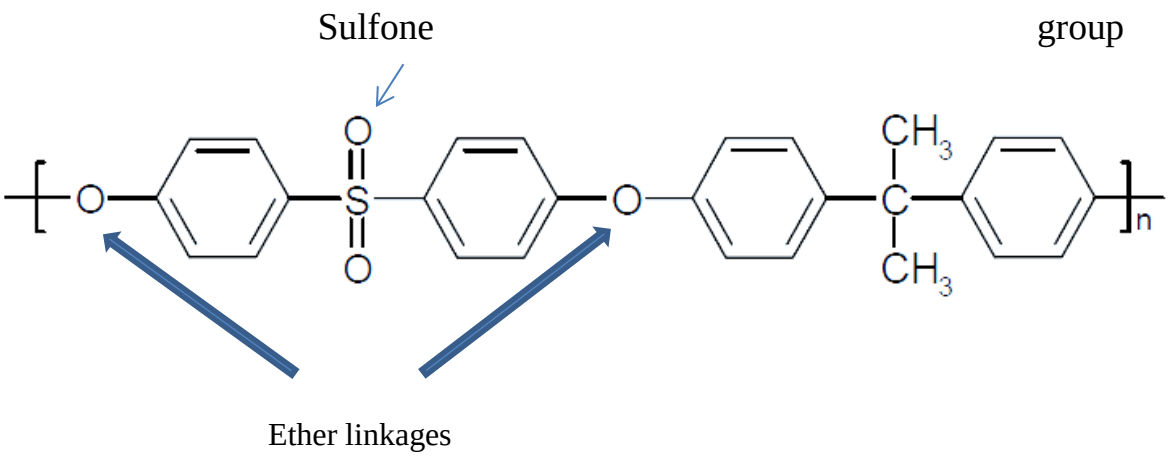

Figure 3. 1 Chemical formula for PES (http://pslc.ws/macrog/pes.htm)

The PVDF (Kynar 740, Arkema Inc., Philadelphia, PA) has been used to prepare the nanofilbers. The acetone and dimethylacetamide (DMAC) used to prepare the electrospinning solution had a purity of at least 99.9%, they were purchased from Sigma-Aldrich (St.Louis, MO).

The proteins used to prepare the fouling test solutions were: trypsin (MW=23.8 KDa); pepsin (MW=35 KDa); egg albumin with a MW of 45 KDa and a purity of 62-88 %; and bovine serum albumin (BSA) with a MW = 66kDa and a purity of 96%. These proteins were also purchased from Sigma-Aldrich (St. Louis, MO). They were selected as the model protein foulants with their intensive fouling affinity which enabled the completion of fouling tests within a limited period of 4 h. Also, a range of molecular weight can be covered by the chosen proteins. A raw Ottawa River water sample was used for an additional fouling test to evaluate the impact of fouling by natural organic matter (NOM). The water quality characterizations in different seasons are provided in Table 3.1. This sample was collected from the intake of the Britannia Water Treatment

Plant in Ottawa, Ontario during the winter of 2015 (Xu, 2015) and in this study only the winter water was used for filtration test. This water has very turbidity, low alkalinity and hardness, thus particulate fouling and scaling are unlikely to be the dominant fouling types. Ottawa River water was selected because it contains a high level of natural organic matter (NOM) and its large hydrophobic NOM fraction (HPO) as 100* HPO/DOC is greater than 70%, and the specific UV absorption (SUVA) is approximately 4. The hydrophobic NOM fraction causes significant fouling (Pezeshk & Narbaitz, 2012). Furthermore, it is typical of northern Canadian waters.

Table 3. 1 ORW quality characteristics in different seasons (Xu, 2015)

Parameters	**Raw ORW**
Season	**Winter**
pH	7.70±0.07
Turbidity (NTU)	3.56±0.06
Alkalinity(mg CaCO3L^{-1})	26.0±0.05
Total Hardness(mgL^{-1})	34.67±3.46
DOC(mgL^{-1})*	8.16±0.06
HPO(mgL^{-1})**	6.33±0.10
SUVA (L$mg^{-1}m^{-1}$)	3.92

*Doc= Dissolved organic carbon;** HPO= Hydrophobic NOM fraction

3.2 Membrane electrospinning

Commercial PES membrane samples were modified by electro-spinning with PVDF nanofibers following the method described by Efome et al. (2016). The spinning dope was comprised of 15% wt PVDF, 34% wt DMAC, and 51% wt acetone. The dope was prepared in a bottle, closed with a cap to prevent evaporation of the solvent, then it was taped tightly and was vigorously

stirred (@180 rpm) for 24 h in an orbital shaker at 50°C. This insured that all the components were well mixed and an uniform solution was produced. Then, the solution was cooled down and kept at room temperature for another 24 h; this process yielded a homogeneous transparent solution.

Finally, the prepared solution was used to produce nanofibers with the electrospinning apparatus (Beijing Ucalery Technology and Development Co., LTD, China) that was located in University of Ottawa laboratory. The picture of the equipment is shown in Figure 3.2. This apparatus has a control panel in the front and the electrospinning chamber in the back.

Figure 3. 2 Electrospinning equipment

Figure 3.3 on the following page shows the inside of the electrospinning box. The arrows in the figure identify some of the key parts of the electrospinning unit. Arrow 1 shows the drum where the commercial PES membrane is attached, (this drum rotates). The apparatus in the center of the image helps form the nanofibers that are deposited on top of the membrane. The system uses a syringe to deliver the small quantities of the PVDF solutions that make up the PVDF nanofibers. Arrow 2 points to the syringe holder (without a syringe). The buttons on the control panel control the movement of the syringe plunger. Arrow 3 identifies the UV lamp used to make the jet of polymer visible while it is extracted from the syringe. And arrow 4 points to the positive electric charge clips for the syringe needle. They help directing the nanofibers to the drum with the negative charge. Note that in this image they are not clipped to the syringe needle as they would be under the normal operation of the system.

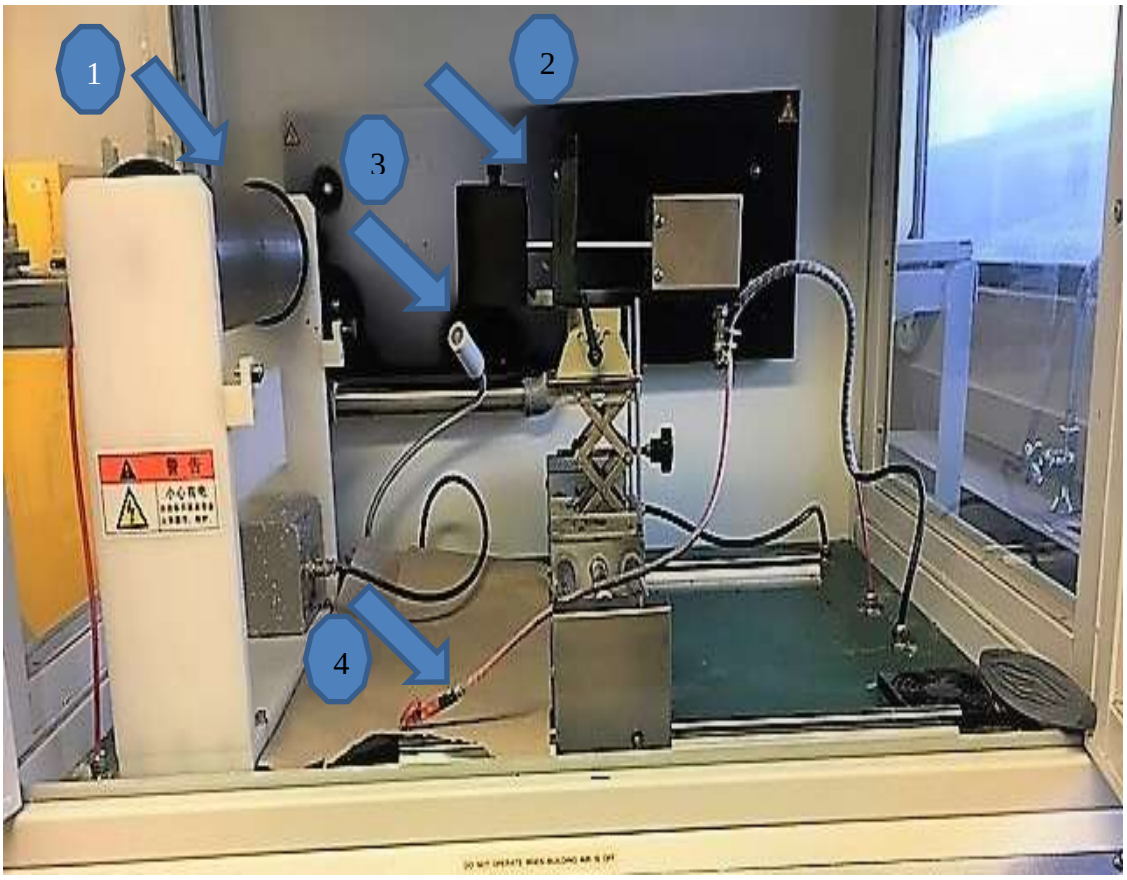

Figure 3.3 Electrospinning chamber

After the PVDF solution was prepared and the equipment was ready for operation, 10 ml of the PVDF solution was loaded into a disposable syringe with a $1.2 \times 40\, mm$ size needle and then placed between the plates in the syringe holder. A commercial flat sheet PES membrane was wrapped around the surface of the drum, which then was rotated at 140 rpm. The needle holder was adjusted so that the distance between the needle tip and the rotating drum was 150 mm. Next, the positive charge clips were attached to the syringe needle and a 15 kV voltage was applied. Then the syringe pump

was started to initiate the electrospinning. The electrospinning was conducted for three different periods: 25, 125, and 250 minutes, which resulted in different thickness electrospun layers on top of the commercial PES membrane.

3.3 Membrane filtration tests

3.3.1 Permeation experiment set-up:

The three cross-flow cells in series membrane filtration set-up used for the experiment are illustrated in Figure 3.4. The system consists of a feed tank (20 litres), a high pressure diaphragm pump (Hydra-Cell, Wanner Engineering, Inc; Minneapolis MN) and the three membrane test cells connected in series.

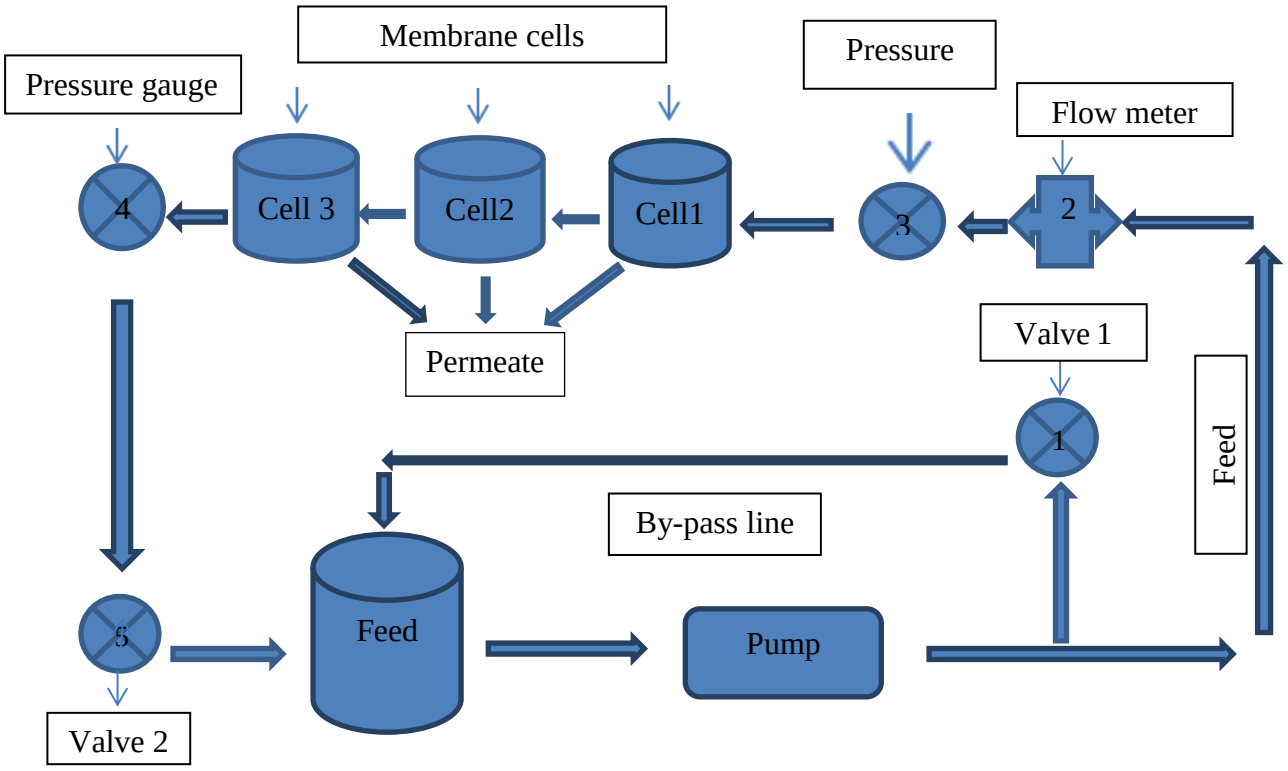

Figure 3.4 Schematic of the filtration system

The flow rate through the test cells was fixed at 1.1 L/min by adjusting the valve in the by-pass line. This flow rate provided turbulent flow (eddies) at the surface of the membranes, which minimized the impact of concentration polarization, and resulted in a small pressure drop along the three cells, approximately [1 psi] or 6.895 kPa (Mosqueda-Jimenez et al., 2004).

The majority of the piping of this system consisted of stainless steel with 3/8" (OD); it connected the pump, the by-pass line, and the test cells. The permeate from the three test cells was returned to the feed tank using 1/8 inch (ID) polyvinyl chloride (PVC) tubing (Nalgene, Lima, OH). The retentate (or concentrate) from the last cell is also returned to the feed reservoir, it flows in a 3/8 in (ID) polyvinyl tubing.

The concentrate and permeate streams were recycled to the feed tank to maintain the concentration of the feed constant. To collect permeate samples for analysis and to measure the permeate flow rates the soft PVC permeate lines were temporarily disconnected and redirected to a sampling beaker. The by-pass in this system was necessary to reduce the high flowrate from the pump outlet (6.8 $Lmin^{-1}$) to the lower feed flow rate that goes through the permeation cells and independently control the feed flow rate from the transmembrane pressure.

The flow rate through the membrane test cells was measured by a flowmeter (P-32025- 20 rotameter, Gilmont Instrument, Barrington, IL). Two pressure gauges (Ashcroft 100 psi Duraguage, Cole-Parmer, Montreal, QC) were used for monitoring the pressures so that the transmembrane pressure of system could be maintained at 345 kPa (50 psi); they are labelled 3 and 4 in Figure 3.4. The system also included two stainless

steel valves (Medium flow metering 31 series, Swagelok, Whitely, OH), valve 1 (in Figure 3.4) was adjusted to maintain the flow rate through the cells at the desired level, while valve 2 (in Figure 3.4) was used for adjusting the transmembrane pressure in the set-up. The UF cells were manufactured in the machine shop oft the engineering faculty at University of Ottawa. They were made of 316 stainless steel and designed based on the recommendations of Sourirajan and Matsuura (1985).

The cross-sectional area of the UF cell is relatively high at the entrance and the exit, which results in a pressure drop of less than 7 kPa (1 psi) across the cell. Also, above the membrane surface is a thin channel (0.6 mm), which results in a high fluid velocity parallel to the surface of the membrane (Mosqueda-Jimenez et al., 2004). They have shown that after running the flow test continuously for six days, the UF cells had a similar flux decline to RO and Sepa CF cells. However, the coupon size used in UF cells was one- eighth of those used in the Sepa CF cells that are recommended by USEPA (Mosqueda-Jimenez et al., 2004).

3.3.2 Permeation and filtration test procedure

The membrane filtration testing procedure consisted of the following phases: pre-compaction, pure water permeation test, fouling test (filtration of either Ottawa River (OR) water or protein solutions), and tangential flow cleaning test. The pre-compaction step consisted of a 4 hr water filtration stage using distilled water as the feed and a 483 kPa (70 psig) transmembrane pressure. This is in contrast to the 345 kPa (50 psig) used in the subsequent filtration tests. The objective of the pre-compaction step was to pre-compact the membrane so that in the subsequent filtration tests the extent of flux decline due to membrane compaction was minimized.

The most critical variable monitored in these tests is the permeate flux (J), i.e. the permeate flowrate per unit membrane area ($Lm^{-2}h^{-1}$). It is calculated as follows:

$$J= V/(A\cdot t) \quad (3.1)$$

Where V is the permeate volume collected (L); t is collection period (h); and A is the effective membrane area (m^2). The membrane area of the cells used in this study was 2.04×10^{-3} m^2 or 20.4 cm^2.

The second phase of the testing was the pure water permeation (PWP) test, that is the filtration of distilled water using the same transmembrane pressure as in the subsequent membrane fouling tests (i.e., 50 psig). This test was conducted immediately after the pre-compaction step by adjusting the valve located downstream of the last membrane cell to reduce the transmembrane pressure from 70 to 50 psig. During this 4 hr test, permeate samples were collected every 30 min to determine the permeate flux.

The PWP test was immediately followed by the filtration/fouling tests. For the latter the feed solution was changed to OR Water or a protein solution of a predetermined concentration. The filtration/fouling phase also lasted 4 h for each protein solution and permeate samples were collected every 30 min to determine the permeate flux. The permeate flux, *J*, was also calculated by equation (3.1). On the other hand, in other studies the filtration tests were performed for less than 4h. For example, Dobosz et al. (2017) and Jamshidi et al. (2013) used 1 and 3.3 h, respectively, for their filtration experiments.

In case of the filtration of the protein solution, the concentration of protein in some of the permeate samples was measured. The solute separation, R, was calculated by:

$$R= 1- \frac{Cp}{Cf} \quad (3.2)$$

Where C_p and C_f are permeate and feed protein concentrations (mgL^{-1}), respectively.

The concentrations of the trypsin, pepsin, egg albumin, and bovine serum albumin in the fouling solutions were approximately 100 mgL^{-1}.

The final phase of the membrane tests consisted of a tangential membrane cleaning/pure water permeation test which was a mild membrane cleaning processes to assess the reversibility of the fouling; also, in this type of cells-in-series filtration system backwashing cleaning was not possible. Immediately after the protein solution filtration step, the feed solution was changed back to distilled water to determine if the tangential flow could help recover permeate flux losses that resulted from the protein fouling. This phase lasted four hours and the permeate flux was determined every 30 min.

After the tangential cleaning step was completed, the next fouling test was performed by switching the feed to the next foulant (e.g., protein) solution and filtering it for four hours. This was then followed by another 4 hr tangential cleaning step. This fouling test – tangential cleaning test sequence was repeated until the impact of all the fouling solutions was evaluated. Accordingly, all of the sets of fouling tests were performed on the same membrane coupons.

It should be noted that numerous membrane coupons were prepared by electrospinning and then tested. They were grouped in a number of "series" and in each series a sequence of experiment, including PWP and filtration/fouling tests, cleaning tests were performed. Prior to testing a new series of coupons, the membrane filtration system was cleaned by using chlorine solution (100-200 mgL^{-1}). The detergent was circulating in the system for 30 minutes while the output tubing was put in the drain instead of the feed tank. This reduces the risk of detergent staying in the system. Then, cleaning was followed by circulating distilled water for three hours and the distilled water discarded. A different sample was then introduced in the system for the subsequent membrane testing.

It should be noted that there are considerable variations in the flux data from membrane sheet to membrane sheet and from coupon to coupon, taken from the same sheet, even though the membrane was purchased from a membrane manufacturer. Normally, the variation from coupon to coupon (from the same sheet) is less than the variation from sheet to sheet. While, in each series of the experiments shown in Table 3.2, the membrane sheets were taken from the same roll of commercial PES membrane. Each control PES sheet was used for the cell coupons and the adjacent sheets were used for different period of electrospinning and then coupons were cut from these electrospun PES membranes to investigate the effect of electrospinning. Thus, the flux variation due to the change in the membrane sheets was greater than variation of coupons.

For instance: in the series 1 experiments the control PES membrane coupon and the coupon on which 250 min of electrospinning was applied (EPES-250) were from the adjacent sheet. When those coupons were tested for ORW fouling, the effect of electrospinning on the flux did not contain the variation due to the difference of the sheet.

Due to the relatively low fouling of the PES membrane in series 1, series 2 switched to filtration/fouling with BSA, to establish if it resulted in more intense fouling than OR water over a four hour filtration period. This proved to be correct and subsequent series of membranes were tested using BSA and other proteins as the foulants. Series 3 evaluated the filtration and fouling of PES membranes and electrospun PES (EPES) membranes prepared with different electrospinning times. Series 4 membranes were prepared and tested to confirm the results of the series 3 tests. The series 5 membranes evaluated the performance of PES and EPES-250 in the filtration of different protein solutions.

Table 3. 2 Experimental plan of this study

Series	Membranes	Type of fouling
Series 1	PES+ EPES-250	PWP+OR fouling
Series 2	PES	PWP+ BSA fouling
Series 3	PES+ EPESs	PWP+ BSA fouling
Series 4	PES+ EPESs	PWP+ BSA fouling
Series 5	PES+ EPES-250	PWP+ proteins fouling

3.4 Analytical Methods

3.4.1 Spectrophotometric Analysis

The concentrations of trypsin, pepsin, egg albumin, and BSA in the fouling solutions were measured using a UV spectrophotometer (DR 6000, Hach Instruments, Loveland, CO). The measurements were conducted at a wave length of 220 nm because they had the better absorbance at this wavelength. The solution was added to a crystal cuvette (1 cm cell path) and the absorbance (Abs) was measured. According to Lambert Beer's law, Abs is proportional to the concentration of the solute, i.e.,

$$Abs = \epsilon \cdot b \cdot c \tag{3.3}$$

Where Abs is absorbance (unitless); ϵ is molar absorptivity (L mol-1cm-1); b is the path length of the sample (cm); and c is the concentration of the compound in solution (mol L-1). Also, absorbance can be calculated with intensity of beam light using the following equation:

$$Abs = \log_{10}\left(\frac{I_0}{I}\right) \tag{3.4}$$

Where, I_0 and I are transmitted intensity of reference blank (distilled water) and the sample, respectively.

The spectrophotometer was calibrated with distilled water and six standards. Distilled water was used to set the absorbance at zero. A 500 mgL^{-1} stock solution was first prepared for each protein and then diluted to obtain a number of standards with different concentrations.

The absorbance values so obtained are given in Table 3.1 for trypsin, pepsin, egg albumin and bovine serum albumin. From the clear linear patterns and the high correlation coefficients, it is evident that there is a linear response between 5 and 100 $mgL^{-1}$for pepsin, egg albumin and BSA. For trypsin, the linear range was 15 to 100 mgL^{-1}.

Table 3.3 Concentration of each protein for UV Calibration

	Absorbance			
Concentration mgL^{-1}	**Trypsin**	**Pepsin**	**Egg album**	**BSA**
5	0	0.031	0.041	0.047
10	0	0.065	0.081	0.104
15	0.011	0.113	0.147	0.157
20	0.022	0.168	0.209	0.213
50	0.089	0.399	0.557	0.637
100	0.193	0.783	1.06	1.342
R^2	0.9997	0.9991	0.9985	0.9992

3.5 Other membrane characterization analysis

The commercial and electrospun membranes were also characterized by scanning electron microscopy (SEM) and contact angle measurements.

3.5.1 Scaning electron microscope (SEM)

A scanning electron microscope, model Vegall XMU (Tescan, Warrendale, PA, USA), located at Carleton University in Ottawa was used to characterize the morphology of the commercial and the electrospun nanofiber PES membranes. Surface and cross sectional images were extracted with different magnifications for each membrane before and after fouling experiments. Detailed information on the samples is provided at the bottom of the images.

After a complete fouling process, which included pre-compaction, fouling, and cleaning with DW, the membranes were dried for two days after being fouled. Each membrane was divided into nine sections, as shown in Figure 3.5, in order to study the effect of flow direction on the orientation pattern of the foulants at the PES and EPES membranes surface. The objective was to determine if the deposited foulant orientation was perpendicular or parallel to the flow direction. In this study, only segments 2, 4, 6, 8 were chosen for the membrane surface investigation by SEM.

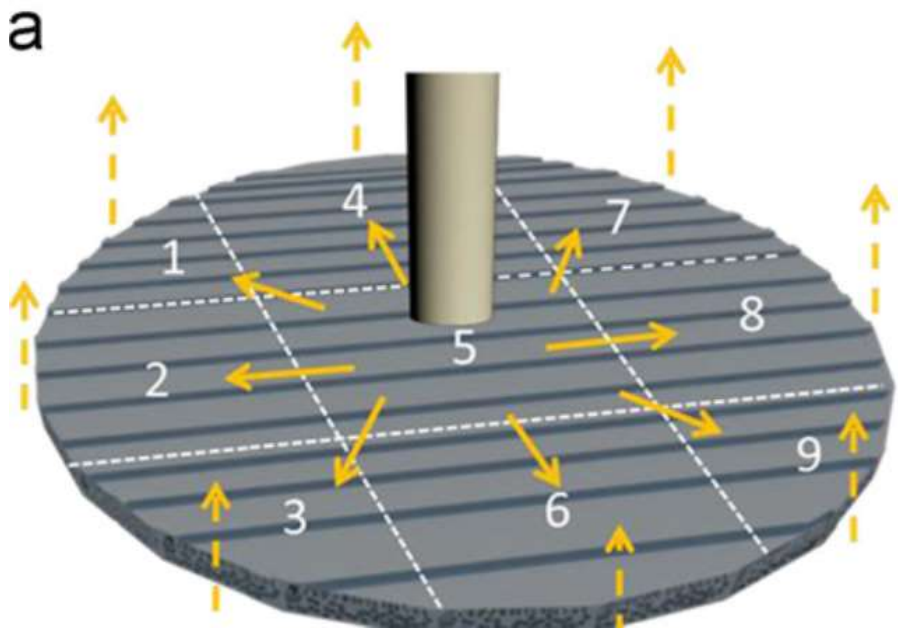

Figure 3.5 Sections of membrane based on the feed flow (Maruf et al., 2013)

Due to the texture of the non-fouled electrospun membrane coupons (that are very soft and had a spider web-like surface), they could be easily damaged; accordingly they were immersed into liquid nitrogen to make them more rigid. Then, it was possible to obtain membrane samples by cutting the frozen coupons with a very small and sharp scissors. The samples were then placed and glued on the SEM holders with the copper foils. In order to increase electron conductivity the samples were coated with gold to a thickness of 10 nm, in a coater (Quorum Q 150T, Britain). The surface and cross section of each membrane sample were studied.

3.5.2 Contact angle measurements

A computer controlled-digital camera based system (VCA Optima Surface Analysis system, AST Products Inc., Billerica, MA) was used to measure the advancing contact angle of the membrane samples (Figure 3.6). Regular and modified membranes were cut into small pieces (10×15 mm) and placed on micro slides (25×75×1 mm) prior to being placed in the analyzer. The analyzer's computer controlled the syringe to gradually pump water into a small droplet on the surface of the membrane, and the analyzer camera continuously monitored the profile of the small droplet as the water was added. The analyzer's software identified when the base of the droplet expanded and at which time it measured the contact angle. The volume of the water droplet used for each measurement with this equipment was 1.5 μL (Pezeshk, 2010). For each sample of membrane contact angle was measured on 20 locations and twice per location and the average was reported.

Figure 3.6 VCA Optima Surface Analysis System

CHAPTER 4

RESULTS AND DISCUSSION

As discussed earlier, several sets of electrospun nanofiber coated polyethersulfone (EPES) membrane coupons were prepared and tested, along with the commercial polyethersulfone membrane coupons (hereafter denoted as PES), each of these sets is referred to as a series. The EPES membranes in these series were produced with different electrospun layer thicknesses and several coupons from the same fabrication series were tested. It should be noted that all coupons were sequentially subjected to 4 h pure water permeation (PWP) test, 4 h fouling tests and followed by 4 h tangential cleaning/ post filtration tests using distilled water. Series 1 tested PES and EPES-250 membranes using Ottawa River water as the foulant solution, series 2 evaluated just the PES membrane with BSA solution as the foulant, and series 3 and 4 tested PES and several thickness EPES membranes using solution of BSA. Also, research was followed with two sets of experiment using solutions of four different proteins for EPES-250 and PES membranes and each fouling stage was followed with the aforementioned 4 h tangential cleaning/ post filtration tests using distilled water, series1 to 4 are provided on further pages in Table 4.1.

This chapter first describes the results of the PWP tests as they were the first stage of each series of filtration tests. Then, the discussion will be followed by the presentation and explanation of the results of each series, including the PWP and filtration results for comparative purposes. Finally, the results of the membrane characterization will be presented.

4.1 Membrane performance testing

4.1.1 Pure water permeation test

Figure 4.1 on the following page shows the pure water permeation fluxes (PWP) as a function of filtration time for the PES membrane and the series 3 EPES membranes prepared with different spinning periods (i.e., 25, 125 and 250 min, hereafter denoted as EPES-25, EPES-125 and EPES-250, respectively). These results are typical of all the series of EPES membranes. As shown in the figure, the PWP fluxes of all the membranes were fairly constant over the four hour test period, they all showed a slight decrease in the flux (less than 7%); however, in some other series of tests the decrease was slightly higher (~10%), from the first hour to the fourth hour. However, conducting a linear regression of the fluxes with time yields a slope whose 95% confidence limits include zero, therefore it can be said that the fluxes are statistically the same over time. Presumably the magnitude of the flux reduction was low because of the pre-compaction step. In addition, EPES membranes of the different series showed significantly different PWP values due to the variability of coupons.

Figure 4.1 also shows that PWP of the EPES membranes were higher than those of the commercial PES membrane without exception, according to regressions and 95% confidence limit. This is quite unexpected since, based on the filtration theory, adding an additional layer will inevitably increase the resistance against the flow across the membrane, causing a decrease in the flux. The magnitude of the flux improvement varied among the different EPES membranes, the flux of EPS-125 was the lowest.

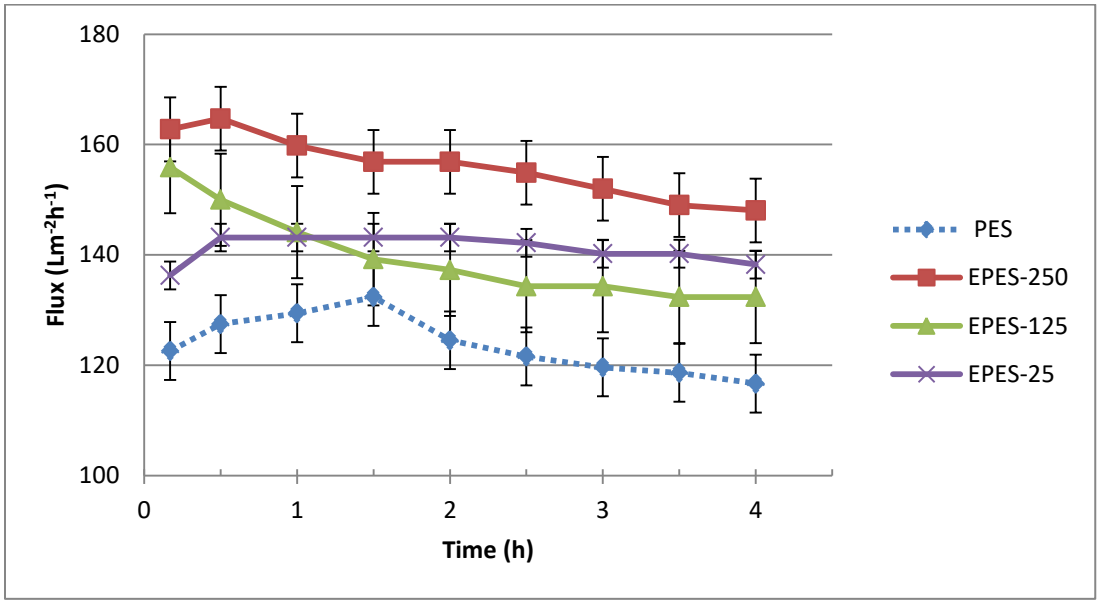

Figure 4.1 PWP flux versus time for a typical set of PES and EPES membranes (series 3)

According to the manufacturer of the commercial PES membrane tested, this membrane has a flux of 287- 442 $Lm^{-2}h^{-1}$ at 25 °C and 50 psi with DI water. The wide range of values is probably due to variability in the membrane manufacturing processes. These values are very high, the lower fluxes measured in this study may be due to the 4

hr pre-compaction step. Table 4.1 presents the PWP data for various types of membranes showing significantly different fluxes for the different membranes coupons tested; for example, in this study the PWP of PES membranes ranged from 66.6 to 127 $Lm^{-2}h^{-1}$. Note that due to uncontrolled factors in membrane manufacturing for all types of membranes, when multiple small coupons of the same type of membrane are tested, there is generally a fairly wide variation in the fluxes (Mosqueda-Jimenez et al., 2004). Moreover, the PWP of the EPES membranes was larger than the corresponding PES coupons, except EPES-125 membrane coupons in series 4.

Table 4.1 PWP of all the series of PES and EPES membrane coupons tested

"Series" [a]	**PWP flux * (L/m^2 h)**		**EPES spinning period (min)**
	PES	**EPES**	
1	66.6	190	250
2	98.6		
3	124	141 140 156	25 125 250
4	127	174 114 242	25 125 250

[a] Membranes in a "series" were used for a series of experiments such as PWP measurement, filtration of OR Water and filtration of protein solutions. Those experiments were conducted upon preparation the of EPES membranes in the series.

[*] Time average flux over the 4 h filtration period and based on three coupons of every type

Table 4.1 shows the significant differences in PWP values between the various series, in order to statistically prove that the EPES membranes indeed had the higher PWP fluxes than the PES membranes a t-test was carried out to confirm that the PWP of the EPES membranes were indeed higher than PES. For this purpose, the data were grouped into variable 1, which includes all the PES data, and variable 2, which includes all the EPES data. First, a t-test was performed assuming equal variances with the null hypothesis that these two groups of data (variables 1 and 2) are from the same sample body. The reason for the assumption of equal variances is that all data were collected with the same PWP experimental protocol. Microsoft Excel® was used to facilitate the statistical data analysis. As shown in Table 4.2, with the degree of freedom 9 (= 11 data points – 2 groups), the t Stat was calculated as -2.59464, which was less than the negative t Critical for one-tail (-1.833113) and the absolute t Stat, 2.59464 is bigger than two-tails (2.262157). Therefore, the null hypothesis was rejected with 95% confidence based on both one- and two-tails. This confirms that the PWP data for EPES came from a different sample body (with larger flux value) than those of PES.

Table 4.2 t- Test: two- Sample Assuming equal Variances

t-Test: Two-Sample Assuming Equal Variances		
	Variable 1	*Variable 2*
Mean	103.7875	165.1543
Variance	769.9753	1750.848
Observations	4	7
Pooled Variance	1423.89	
Hypothesized Mean Difference	0	
df	9	
t Stat	-2.59464	
P(T<=t) one-tail	0.014496	
t Critical one-tail	1.833113	
P(T<=t) two-tail	0.028992	
t Critical two-tail	2.262157	

It is difficult to know why the PWP increased with the coating of the hydrophobic nanofiber layers, as the additional layers increase the membrane thickness and theoretically it should increase the resistance to water flow and the flux should decrease. In this regard, it is interesting to note that while this work was being undertaken Dobosz et al. (2017) reported that the pure water flux of a polysulfone substrate membrane was enhanced (35%) when coated with polysulfone nanofiber but not when cellulose nanofibers were used. Since polysulfone is more hydrophobic than cellulose, their work implies that nanofiber should be sufficiently hydrophobic to induce the flux enhancement. Considering that PVDF nanofibers were used in our work for electro-spinning are more hydrophobic than polysulfone, the results of this thesis corroborate the findings of Dobosz et al. (2017).

A number of mechanisms were considered to explain the observed flux enhancement. One was that the surface morphology of the PES substrate was changed by the electro-spinning. This possibility was, however, disproved by experiments with membranes processed in the electrospinning apparatus with a solvent spray without polymer; these membranes did not show a PWP enhancement (Appendix A). It is likely that solvent evaporated completely while extracting from the syringe and did not reach the collecting drum. A second possibility might be that the modified PES membranes become stronger due to the electrospun layer, so there is less compaction, deformation, and ultimately, narrowing of the pores of the PES membrane and reducing its fluxes.

Finally, the electrospun layer is a more hydrophobic layer and consists of larger pores compared to the PES support membrane; therefore, the pores may provide a channeling of the flow through the membrane resulting in less fluid friction and higher fluxes through the EPES membranes.

4.2 Series 1 Tests including filtration of Ottawa River (OR) Water

Series 1 tests evaluated PES and EPES-250 membrane samples (Table 4.1) and the procedure included a PWP test, followed by a filtration/fouling tests with Ottawa River water and a 4 hr tangential cleaning/filtration test. The results of the PWP experiments are shown in Figure 4.2. It should be noted that three coupons were taken from each membrane sheet and the average value is reported. From the figure it is evident that the PWP flux of the EPES-250 membrane decreased gradually with time but it remained approximately three times higher than that for the PES membrane. The PWP flux of the PES membrane was stable during the entire 4 h period; this has been confirmed by the flux versus time linear regression results. That is, the regression yielded 95 % confidence limits of the slope which included zero, so, statistically it can be said that the flux did not change with time.

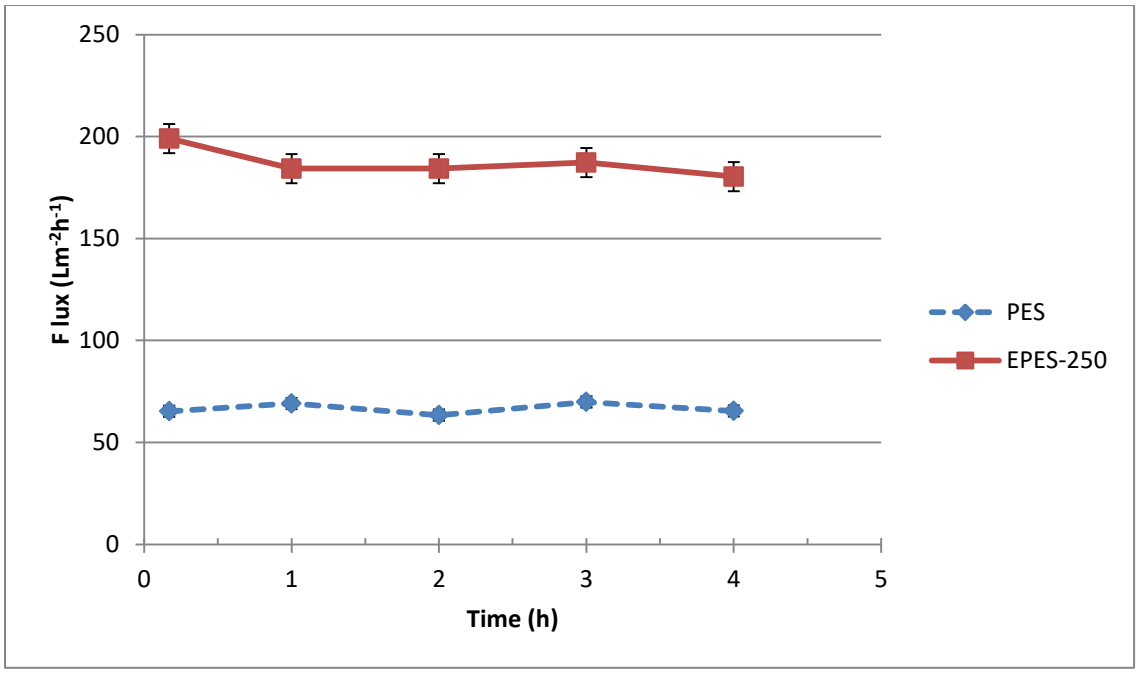

Figure 4.2 Change of PWP flux during the PWP experiments with time for Series 1 PES and EPES-250 OR filtration test

The apparent decrease in the flux of the EPES-250 membrane over time suggests that the PVDF electrospun layer on the EPES-250 membrane was more compressible than the support PES membrane. However, the linear regression of the EPES-250 flux versus time data yielded that the confidence limits of the slope included zero, so the flux decrease is not statistically significant.

The PWP tests (using distilled water as feed) were followed by the filtration/fouling tests with OR water as feed. Figure 4.3 shows that the initial permeate flux of EPES-250 membrane for OR water (J = 140 $Lm^{-2}h^{-1}$) was much lower than the PWP at the end of the PWP test (J_{pwp} = 180 $Lm^{-2}h^{-1}$ as seen in Fig. 4.2) and it kept decreasing with time. In contrast, the permeate flux of PES was only slightly lower than

that in the PWP test and it was stable. Nevertheless, the permeate flux of EPES-250 was significantly higher than PES during the 4 hr filtration period. In retrospect, longer fouling tests would have been desirable.

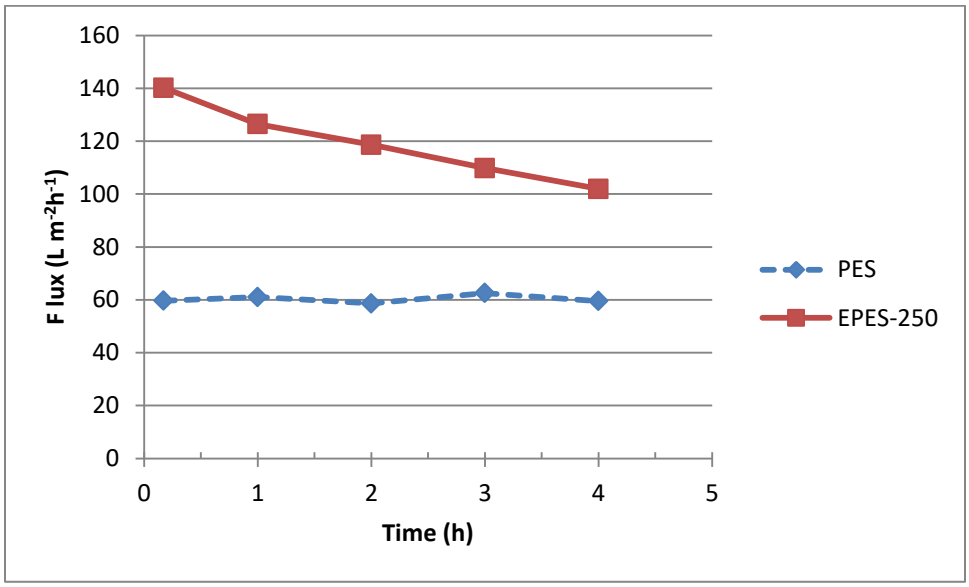

Figure 4.3 OR Water permeate flux for Series 1 PES and EPES-250

The constant flux for the PES membrane implies that the NOM in Ottawa River water did not significantly foul the PES membrane. This was rather surprising because the figures in Dang et al. (2006) had significantly higher flux decrease (approximately 70% decrease) in the treatment of OR water over a longer period of testing using several commercial PES membranes.

The EPES-250 showed a significant decrease in flux with time, this decline appears to be associated with the fouling of the void spaces within the electrospun layer or on the top surface of the electrospun layer. This hypothesis is possible because of two points. First, the hydrophobic fraction of the natural organic matter within Ottawa River water accounts for 77.6 % of the organic matter (Xu, 2016) and its hydrophobic nature

makes it more likely to adsorb onto surfaces. Second, the more hydrophobic characteristics of the PVDF nanofibers compared to the PES in the support membrane will theoretically result in greater adsorption and thus accumulation on the surfaces of the PVDF nanofiber layer.

The final step of the Series 1 membranes was the tangential cleaning – filtration step with distilled water as feed. The turbulence created by the feed, which travels tangentially to the membrane surface, is expected to remove foulants from the surface of the membrane and thus allow the flux to increase with time. Figure 4.4 shows the effect of cleaning with distilled water filtration. EPES-250 showed a remarkable flux recovery but did not reach PWP flux at the end of the first PWP test (J_{PWP} =180 L $m^{-2}h^{-1}$). So presumably some of the OR foulants accumulated within the nanofiber layer out of the reach of the tangential flow. The flux of the PES membrane, which presumably was not significantly fouled, had a fairly constant flux which was only slightly lower than the PWP (J_{PWP} = 66.6 L $m^{-2}h^{-1}$).

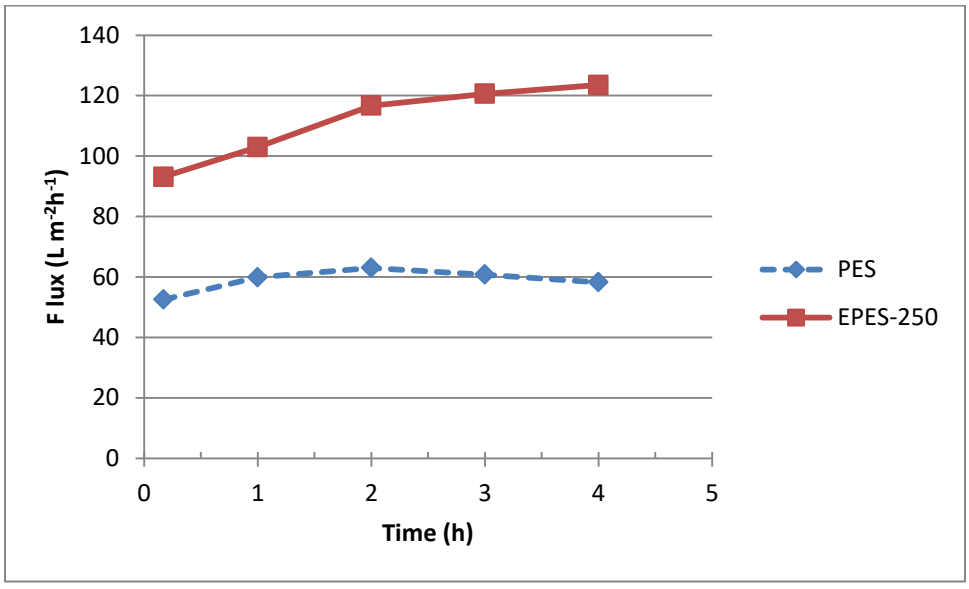

Figure 4.4 Change of PWP flux during the second PWP/tangential wash tests for Series 1 PES and EPES-250

4.2.1 Filtration of protein solutions

4.2.1.1 Filtration of a BSA solution with series 4 PES and EPES membranes

The first protein fouling test was conducted with BSA solutions for all the series 4 PES and EPES membranes and the results are shown in Table 4.3. There are differences in the BSA fluxes among the three coupons of each type that were tested. The variability in the fluxes was quantified using the coefficient of variation, i.e., the percent of the standard deviation divided by the mean. In these tests this parameter ranged from 1 to 9 percent based on three coupons of the same type of membrane. It is likely that this variability in the fluxes arises due to differences in the coupons tested. Therefore, the reported values are the average of all the flux data obtained for a particular membrane. In this table, the average flux of the PES is lower than those of the EPES membranes, however, only the fluxes of the EPES- 25 membrane coupons were statistically different at the 95% confidence level from that of the PES membrane. This is in contrast to the PWP fluxes of the EPES membrane in this series, which had significantly different PWP fluxes from those of the PES membrane coupons. The difference in the flux of the EPES-250 and EPES- 125 was very small (91.5 L $m^{-2}h^{-1}$ (LMH) versus 98.9 L $m^{-2}h^{-1}$ (LMH), respectively).

Table 4.3 Average permeate flux of series 4 membranes with the BSA solution

Membrane	PES	EPES- 250	EPES- 125	EPES- 25
Average Fouling Flux * L $m^{-2}h^{-1}$	84.3	91.5	98.9	102
Standard deviation	3.5	5.57	4.41	2.76

* Time averaged permeate flux is based on the 4 h filtration of 3 coupons

Images of fouled PES and EPES-250 after BSA fouling tests are shown in Figure 4.5. The nanofibers become dense gelatinous material and dry immediately when they were exposed to the air.

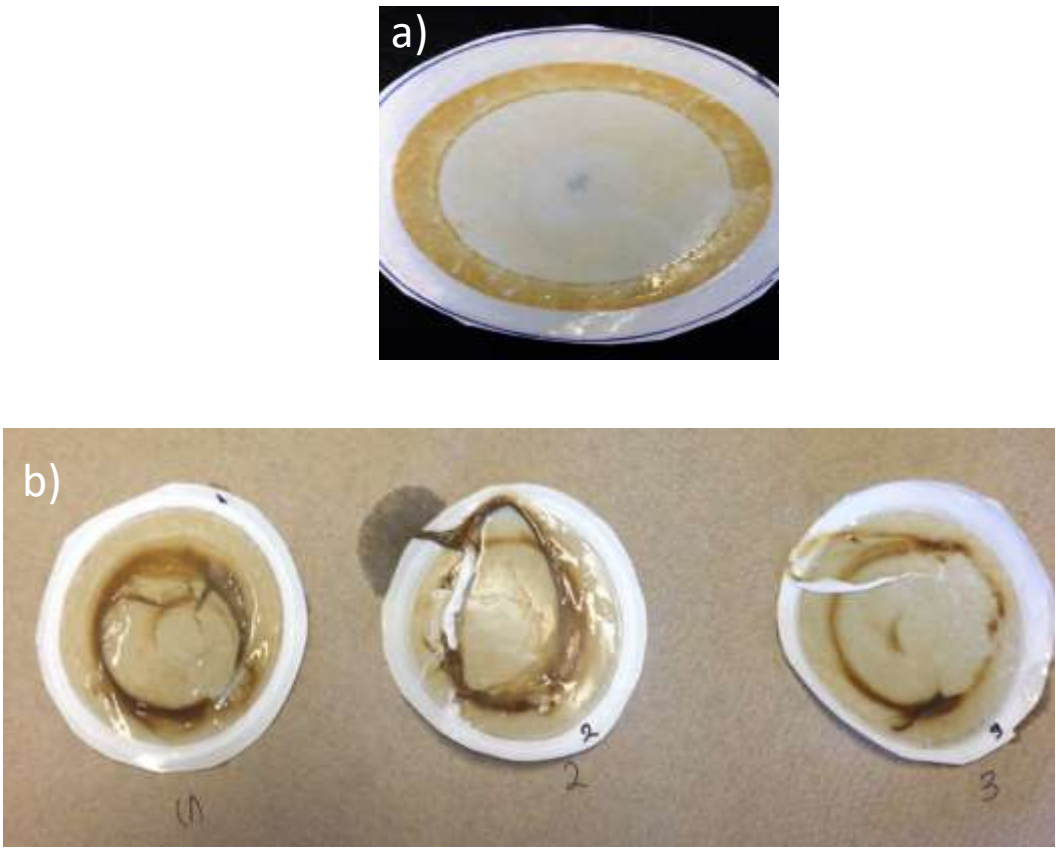

Figure 4. 5 Images of fouled a) PES and b) EPES-250 with the cells area of 20.4 cm^2 and after BSA fouling test

Figure 4.6 shows the decreasing trend of BSA filtration fluxes from PES to EPES-250. The difference of average BSA flux for PES and EPES-250 is lower than PES with other EPES membranes.

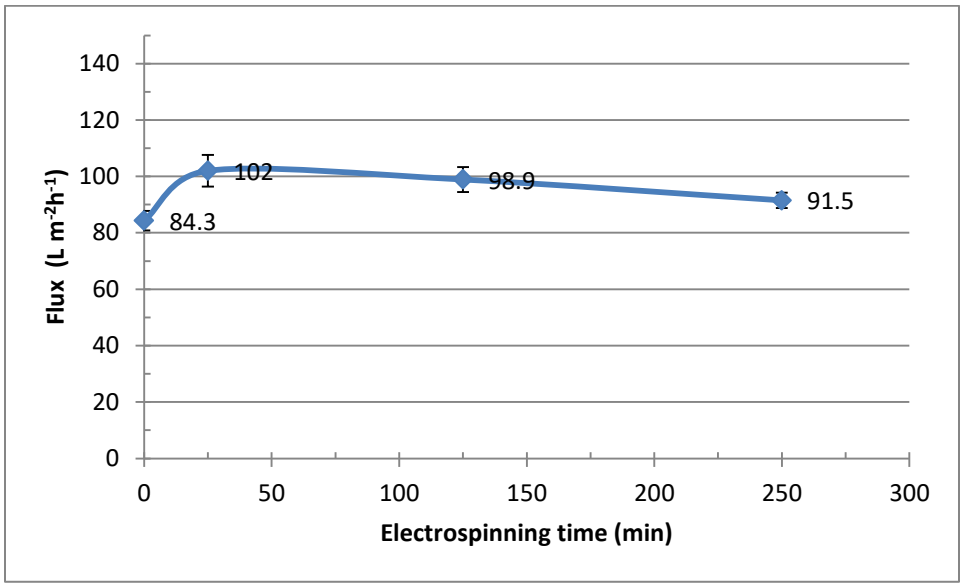

Figure 4.6 BSA filtration fluxes for membrane series 4

Also, it should be noted that permeate fluxes decreased sharply from those during the PWP cycle to the first flux measurement for BSA filtration tests and remained statistically constant for the 4 hrs of the test. For example, PWP flux for EPES-250 was 242 L m^{-2} h^{-1} and it decreased to 91.5 L m^{-2} h^{-1} during the fouling test. Due to the rapid fouling one could hypothesize that the fouling was presumably caused by the sorption of the proteins on the electrospun PVDF layer, which has hydrophobic characteristics.

The percentage of flux reduction of each membrane has been calculated with equation 4.1 and they are presented in Table 4.4.

$$\% \text{ Flux Reduction} = [(J_{PWP} - J_{BSA}) / J_{PWP}] \times 100 \quad (4.1)$$

Where, J_{BSA} is the average flux of BSA filtration for the three coupons averaged over time.

Table 4. 4 Flux reduction percentage of BSA fouling test for membranes series 4

Membrane	**PES**	**EPES- 250**	**EPES- 125**	**EPES- 25**
Average Fouling Flux L m^{-2} h^{-1}	84.3	91.5	98.9	102
% Flux Reduction	33.6	62	13	41

Table 4.4 shows that the PES membrane has a lower percent flux reduction compared to the EPES- 250 and EPES- 25 membranes. However, EPES- 125 shows a different trend and its flux reduction is the lowest among all four membranes. In addition, if the fouling was associated with the penetration of the foulant within the PVDF nanofiber layer, one would expect that the degree of flux reduction would be proportional to the PVDF nanofiber layer thickness. However, due to the low PWP of the EPES-125, there was no clear trend between the flux reduction and the PVDF layer electrospinning time that controls the layer thickness.

4.2.1.2 Fouling of series 4 PES and EPES-250 membranes by various protein solutions

Considering the scatter among different coupons and the change with time of PWP (as well as the permeate flux of protein solutions), the fluxes of the PES and EPES-250 membranes, as the main focus of this study, are compared in Table 4.5 based on the average PWP flux during the entire 4 h period together with the standard deviation (S) and the 95 % confidence intervals (average ± 1.96S) (Montgomery & Runger, 2011). This table shows that: a) the PWP fluxes of PES and EPES-250 are statistically different at the 95% confidence limits do not overlap; b) the fluxes were fairly constant as the standard deviations are significantly smaller than mean values.

Table 4.5 PWP data for Series 4 PES and EPES-250

Membrane	PES	EPES-250
Average Flux ($L\ m^{-2}\ h^{-1}$)	127	242
Standard deviation ($S, L\ m^{-2}\ h^{-1}$)	5.07	9.95
A+1.96S ($L\ m^{-2}\ h^{-1}$)	137	261
A-1.96S ($L\ m^{-2}\ h^{-1}$)	117	222

Next, the Series 4 PES and EPES-250 membrane coupons were subjected to filtration tests with solutions of different proteins, the permeate flux data for each protein solution are presented in Table 4.6.

Table 4.6 Permeate Flux of Series 4 PES and EPES-250 membrane coupons for the various feed protein solutions

Protein	**Trypsin (MW 2300)**		**Pepsin (MW 34500)**		**Egg albumin (MW 42700)**		**BSA (MW 67000)**	
Membrane	PES	EPES-250	PES	EPES-250	PES	EPES-250	PES	EPES-250
Average Flux (A), (L m^{-2} h^{-1})	92.2	127	82.4	108	78.4	93.5	84.3	91.5
Standard deviation (SD), (L m^{-2} h^{-1})	1.70	14.8	1.96	3.96	1.70	4.08	3.5	5.57
A+1.96S (L m^{-2} h^{-1})	95.5	156	86.2	116	82	101	91.2	102
	↕	↕	↕	↕	↕	↕	↕	↕
A-1.96S (L m^{-2} h^{-1})	88.8	98.2	78.5	100	75.1	85.5	77.5	80.6
% Flux Reduction (Cumulative)	27	47	35	55	38	61	34	62

A= average flux

Comparing Tables 4.5 and 4.6, the average permeate fluxes with the protein solutions as feed are much lower than the PWP, 27- 38 % lower for the PES membrane and 47- 62 % lower for the EPES-250 membrane. Table 4.6 shows the flux of the EPES-250 membrane coupons are higher than that for the PES membrane coupons for each of

the protein solutions tested. Only for BSA there is an overlap in the 95% confidence limits of the fluxes of the PES and EPES-250 membranes, the PES and EPES-250 membrane fluxes for the other protein solutions are statistically different.

As well, the fluxes decrease progressively from Trypsin to BSA as the molecular weight of protein increases. This phenomenon is likely due to fouling by the solute protein, consideration of the higher PWP of EPES than PES, and the severer pore blocking by the larger protein.

4.2.2 Analysis of fouling by OR Water

The OR water fouling data shown in Figures 4.2, 4.3 and 4.4 were further analyzed to determine the flux decrease due to compaction (*Comp)*, due to the total fouling (R_{total}), irreversible fouling (R_{irr}), and reversible fouling (R_{rev}). These parameters were calculated using equations 4.3 to 4.5 which were adopted from Kanagaraj et al., 2014. Those parameters are defined as,

$$Compac = (Jw_0 - Jw_1)/J_{w0} \quad (4.2)$$

$$R_{total} = (Jw_1 - Jp)/Jw_1 \quad (4.3)$$

$$R_{irr} = (Jw_1 - Jw_2)/Jw_1 \quad (4.4)$$

$$R_{rev} = (Jw_2 - Jp)/Jw_1 \quad (4.5)$$

Where:

Jw_0: The first pure water flux ($Lm^{-2}h^{-1}$)

Jw_1: The last pure water flux ($Lm^{-2}h^{-1}$) before the fouling experiment

Jw_2: The last pure water flux ($Lm^{-2}h^{-1}$) of post fouling experiment

Jp: The last flux ($Lm^{-2}h^{-1}$) with OR Water (i.e., the fouling test)

Compac: Fractional flux reduction by compaction based on Jw_0

R_{total}: Fractional flux reduction due to both irreversible and reversible fouling based on Jw_1, i.e., it equals $R_{irr} + R_{rev}$

R_{irr}: Fractional flux reduction due to irreversible fouling based on Jw_1

R_{rev}: Fractional flux reduction due to reversible fouling based on Jw_1.

As aforementioned, tangential cleaning, a rather cleaning process was applied in this study since the filtration system did not allow performing membrane backwashing. Thus, the reversible flux reduction calculated by R_{rev} is conservative as more intensive cleaning methods (such as backwashing) and chemical cleaning methods will yield smaller R_{irr} values and therefore larger R_{rev} values.

The values of these parameters for the series 1 are summarized in Table 4.7.

Table 4.7 Normalised flux decrease of Series 1 PES and EPES-250 by OR Water due to compaction and fouling

Parameter	PES	EPES-250
Compac	0	0.094
R_{total}	0.09	0.43
R_{irr}	0.11	0.32
R_{rev}	-0.02	0.12

From Table 4.7 it is evident the reduction of PES by compaction was not significant because compaction value for PES is zero which indicates that there is no difference between the initial PWP flux and the last one during the PWP stage. The total flux reduction for the PES membrane is relatively small, which was expected due to the relatively small flux decrease. This fouling was mostly due to irreversible fouling. The negative value of R_{rev} for the PES membrane means J_{w2} was slightly lower than J_p. Flux reduction parameters for the EPES-250 membrane indicate that a much greater fraction of the flux reduction was due to compaction and fouling.

The greater role of compaction is possibly due to the softness of the nanofiber layer. Due to the more stagnant OR water within the nanofiber layer, concentration polarization will be greater with the EPES membranes than the PES membrane and likely causes the observed greater flux reduction. Some of the foulants are deposited on the nanofiber layer, causing severe irreversible fouling, which was also observed by Gopal et al. (2006).

4.2.3 Analysis of fouling by the BSA solution

Finally, the fouling analysis using equations 4.2 to 4.5 was repeated for the experiments using the BSA solution with the Series 3 PES and EPES membranes prepared with various electro-spinning periods (Table 4.8). The flux data for these calculations were presented in Table 4.8. It should be noted that *Jp* in equations (4.3) and (4.5) is now the last permeate flux measurement for the protein feed solution.

Table 4.8 Flux reductions by compaction and BSA fouling for Series 3 PES and EPES membranes of different electro-spinning periods.

	PES	**EPES-25**	**EPES-125**	**EPES-250**
Compac	0.05	<0	0.15	0.09
R_{total}	0.15	0.52	0.68	0.52
R_{irr}	0.03	0.52	0.54	0.44
R_{rev}	0.13	0.00	0.14	0.07

As the Compac is determined based on the initial PWP stage it is independent of the foulant that is used. So, for the PES and EPES-250 membranes the Compac values for these experiments and those presented in Table 4.7 should be the same. The Compac values for the EPES-250 are almost the same (0.09 versus 0.094), but for the PES coupons there was a slight increase (0 in Table 4.7 to 0.05 in Table 4.8).

The difference may be due to coupon variability. Also, the Compac value increased as the electro-spinning period increased from EPS-25 to EPS-125. According to Table 4.8, a very small negative Compac was calculated for EPES-25, this occurred

because the final PWP flux was slightly higher than the initial PWP flux. Flux reduction by fouling (R_{total}) is more severe for the EPES membranes than the PES membrane, as expected because of the trapped foulant on the surface of EPES membranes. The fouling of the PES membranes was primarily reversible as R_{rev} was 0.13 while R_{total} was 0.15. The fouling of the EPES membranes was also primarily irreversible as the ratio of R_{irr} to R_{total} were 1, 0.79 and 0.85 for the EPES-25, EPES-125 and the EPES-250 membranes, respectively.

4.3 Membrane characterization

The membranes used in this study were characterized by scanning electron microscope imaging, contact angle measurements and pore size distribution characterization.

4.3.1 Scanning electron microscopic (SEM) image analysis

Figures 4.7 and 4.8 on the following page show the membrane surface SEM images of PES and EPES-250, respectively, the a) images are for the virgin membranes and the b) images are for membrane coupons after the filtration experiments with OR Water (and the subsequent tangential cleaning/filtration step). Figures 4.7 a) and 4.8 a) show the surface images of the PES and EPES-250 membranes, respectively, before the OR Water filtration test performance. The PES membrane is relatively smooth, while the EPES-250 membrane's surface is covered by electro-spun nanofibers with a small number of beads.

The space between the fibers appear to be much larger that the diameter of the fibers. Comparing the surface of the virgin PES membrane (Figure 4.7 a) with the surface of the PES membrane post OR water fouling there appears to be a wavy pattern. This could possibly be created by the flow of the feed OR Water. The surface SEM images of the virgin and fouled EPES- 250 membranes are presented in Figure 4.8 a) and b), respectively. The surface of the fouled EPES-250 surface is uniformly covered by foulants without showing any patterns and significantly fewer fibers remain visible, the foulant seems to have partially filled the voids in between the nanofibers. In addition, SEM images showed that the morphology and orientation pattern of membranes sections are not affected by the flow direction.

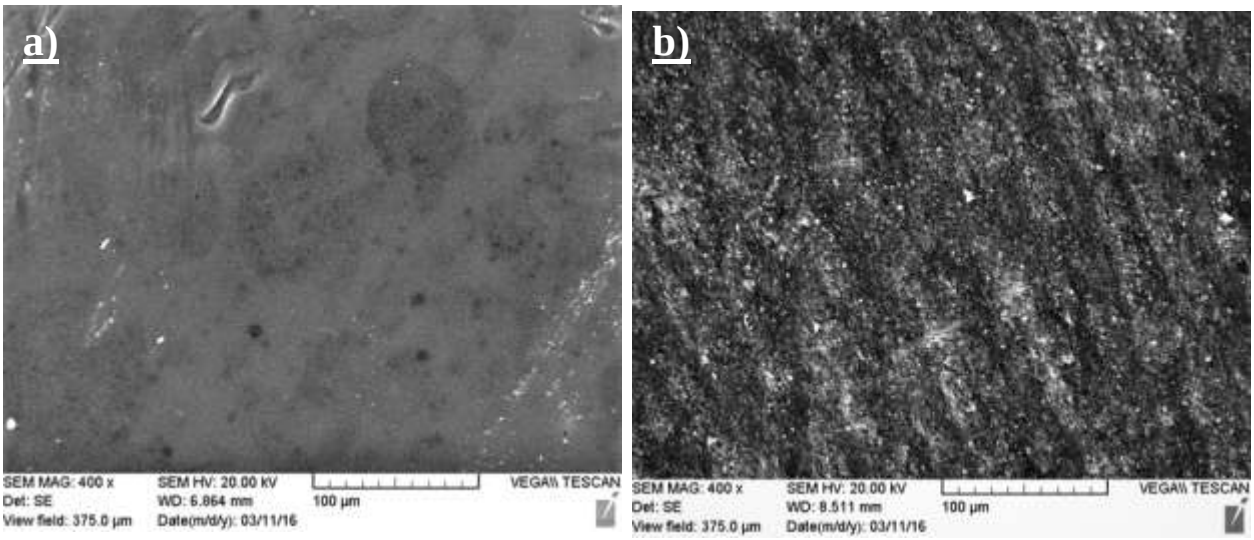

Figure 4.7 SEM surface image of a) PES before and b) PES after the filtration of OR Water and cleaning

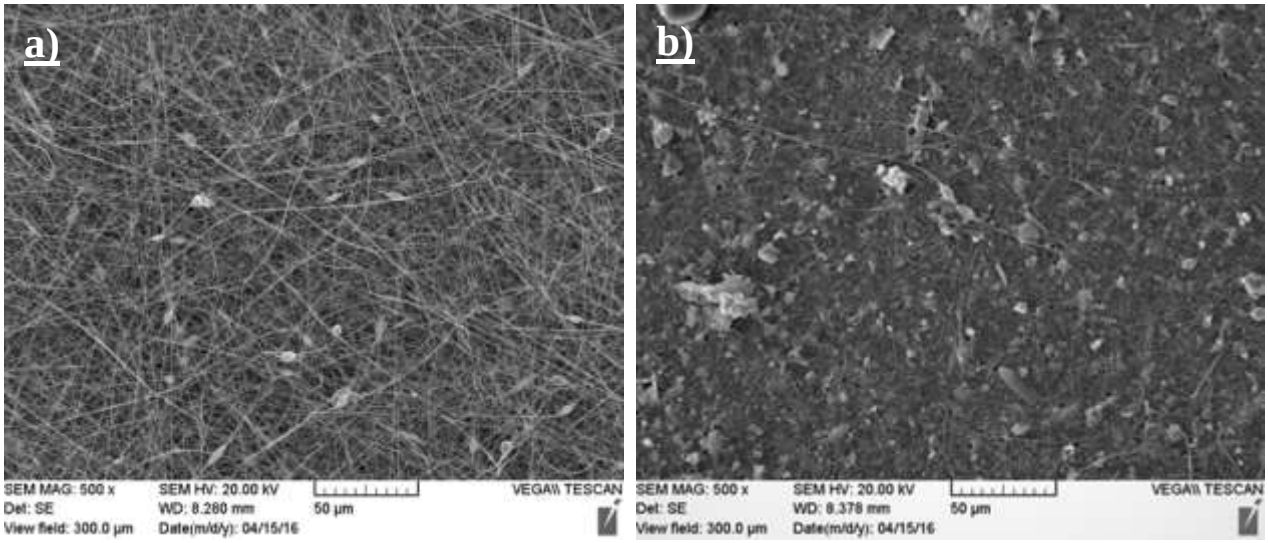

Figure 4.8 SEM image of a) EPES-250 before and b) EPES-250 after filtration of OR Water and cleaning

The magnification of the SEM images was changed from PES to EPES to show the contrast of the surface morphologies of these two membranes distinctively.

A clearer image of the PES membrane surface was taken by higher magnification (Figure 4.9), allowing the identification and measurement of foulant spheres. As shown in the figure, the diameters of large spheres were slightly less than 1 μm and they may be bacteria, as many spherical bacteria are around 1 μm in diameter.

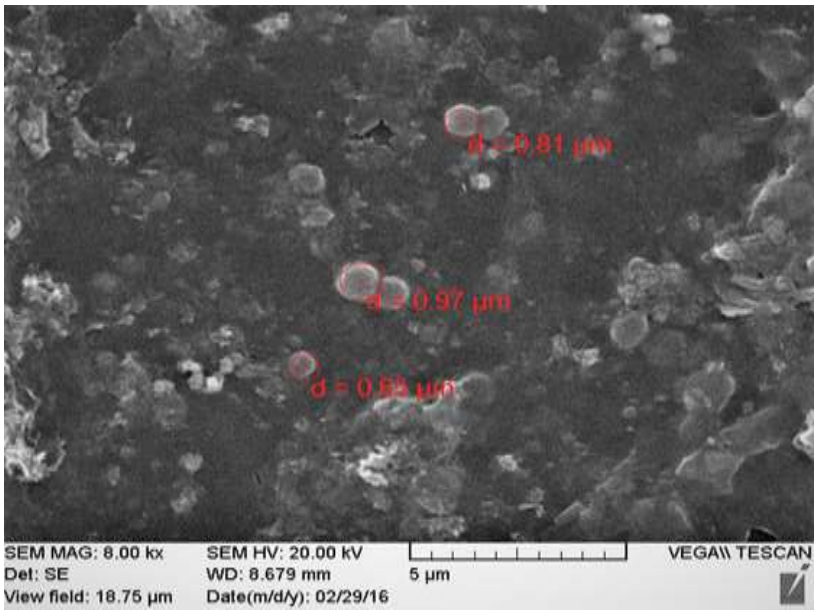

Figure 4.9 8K magnification SEM image of the surface of the PES membrane fouled with Ottawa River water

Figure 4.10 and 4.11 on the following page present cross-sectional images of the PES and EPES membranes. Figure 4.10 a) shows the asymmetric structure of the PES substrate with a skin layer at the top surface prior to filtration and Figure 4.11 a) shows the electro-spun nanofiber layer coated on top of the PES substrate prior to filtration. Figure 4.10 b) shows a higher magnification image of the cross-section of the PES membrane after OR water filtration; it shows the support layer, the thin separation layer with a significant lighter colour layer of foulant above it. Figure 4.11 b) shows a higher magnification image of the nanofiber part of the EPES-250 membrane; it shows that some foulant particles were trapped between fibers of the electro-spun nanofiber layer. Foulant particles can be distinguished from the nanofiber beads in Figure 4.11 b) as particles are more round than nanofiber beads.

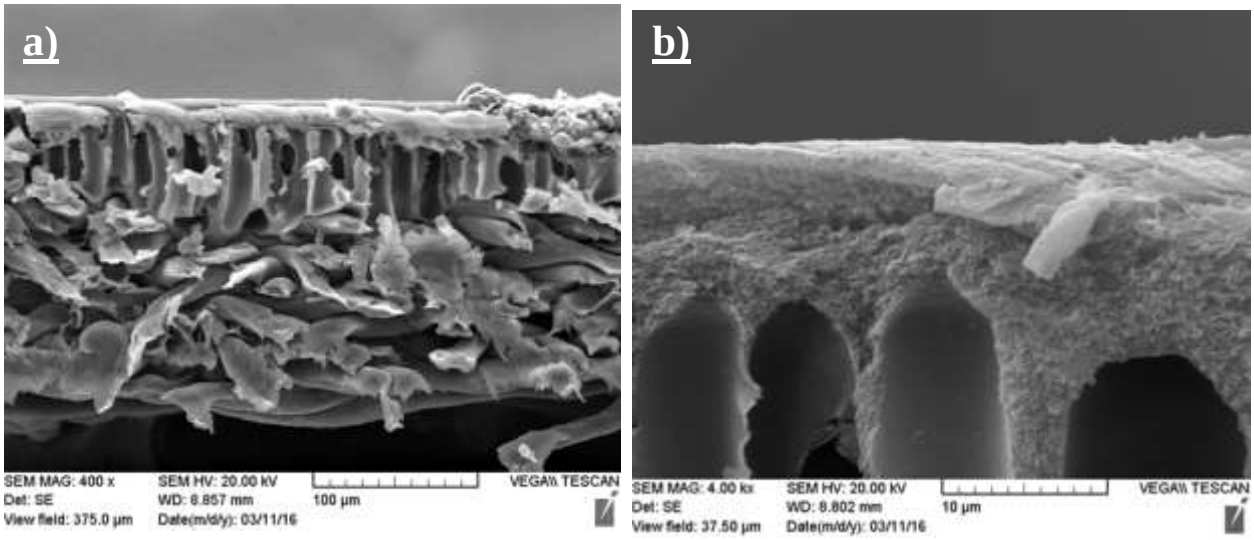

Figure 4.10 Cross-sectional images of a) PES membrane before filtration; b) PES membrane after filtration of OR Water and cleaning

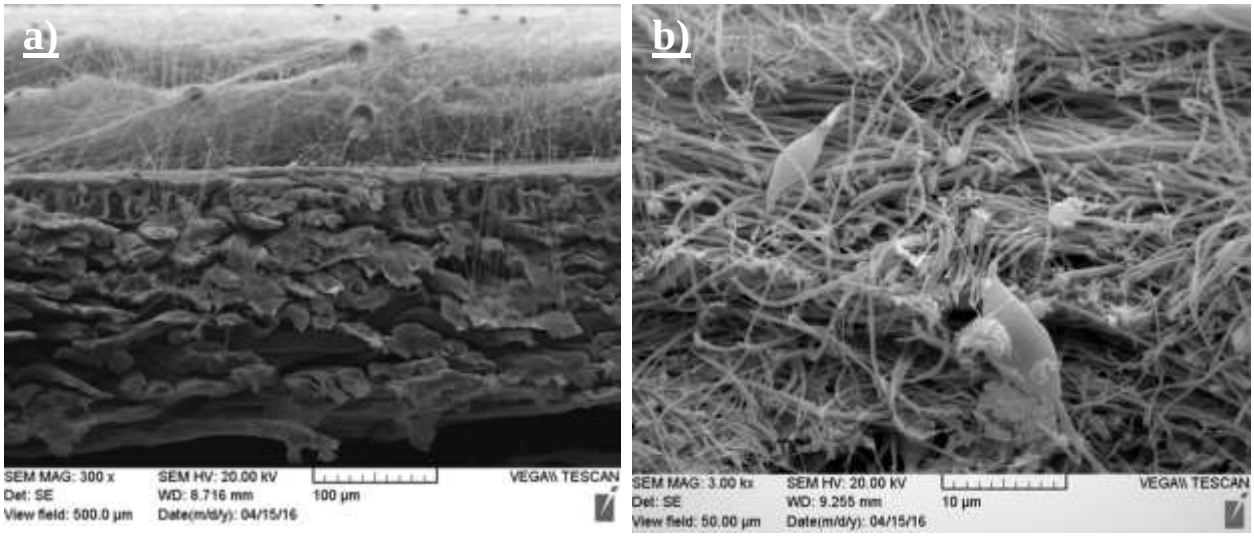

Figure 4.11 Cross sectional images of a) EPES-250 membrane before filtration; and b) EPES-250 membrane after filtration of OR Water and cleaning

Figures 4.12, 4.13 and 4.14 are the cross-sectional images of virgin EPES-25, EPES-125 and EPES-250, respectively. In the figures a) and b) are the lower and the higher magnification images of the membranes, respectively. The (b) images show typical examples for the thickness measurement of the electrospun nanofiber layer. Based on the images of 5 to 7 different measurements, the thickness of the nanofiber layer ranged 8 to 16, 19 to 56 and 89 to 93 μm for EPES-25, -125 and -250, respectively.

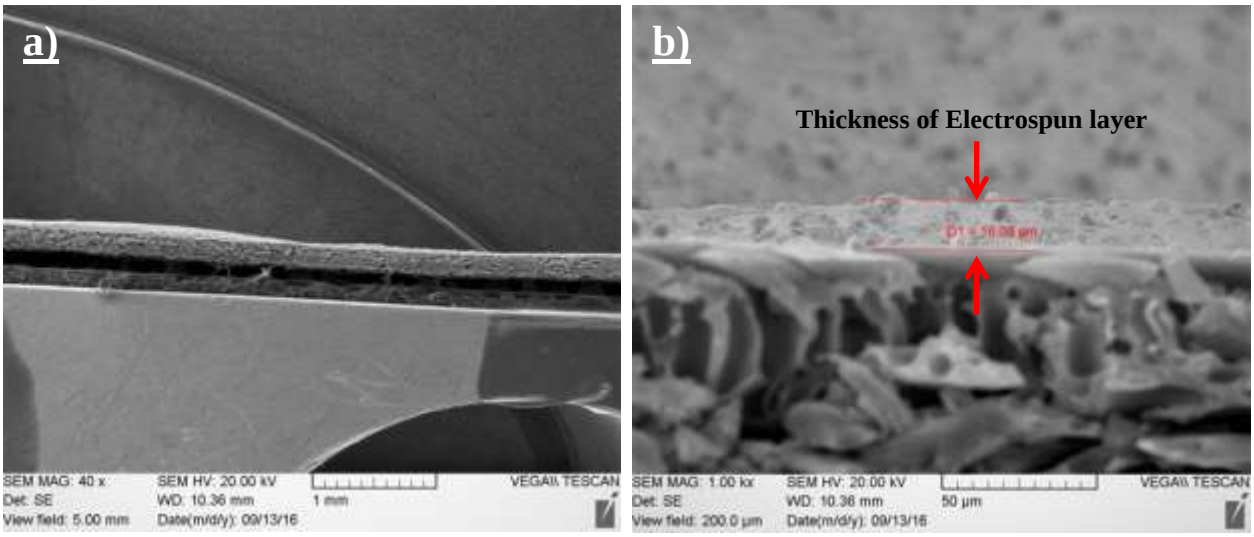

Figure 4. 12 Cross-sectional images of the virgin EPS-25 membrane

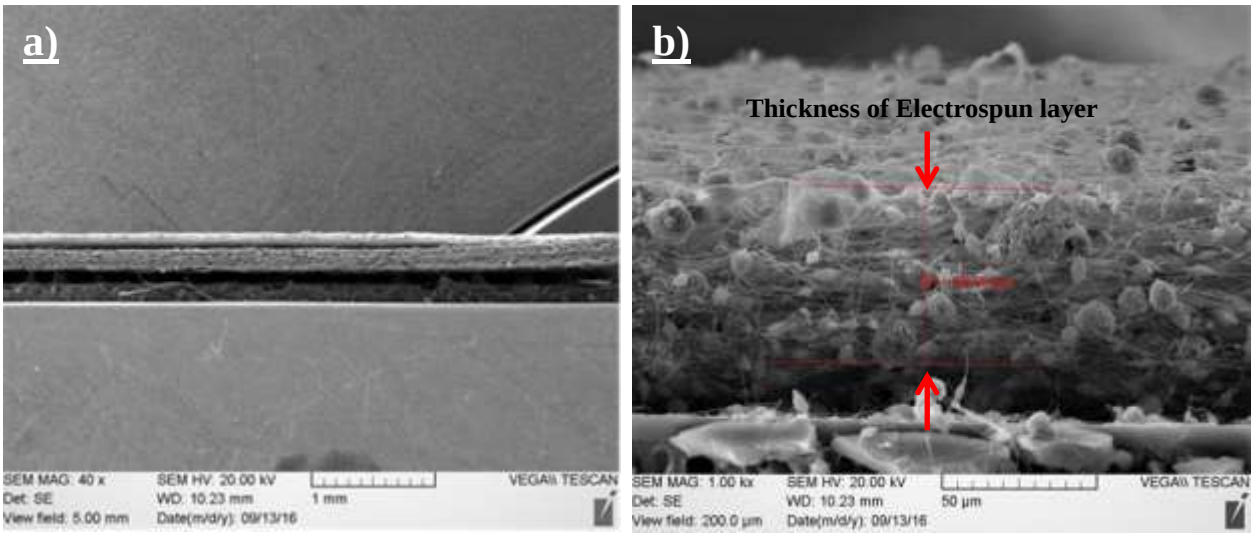

Figure 4. 13 Cross-sectional images of virgin EPES-125 membrane

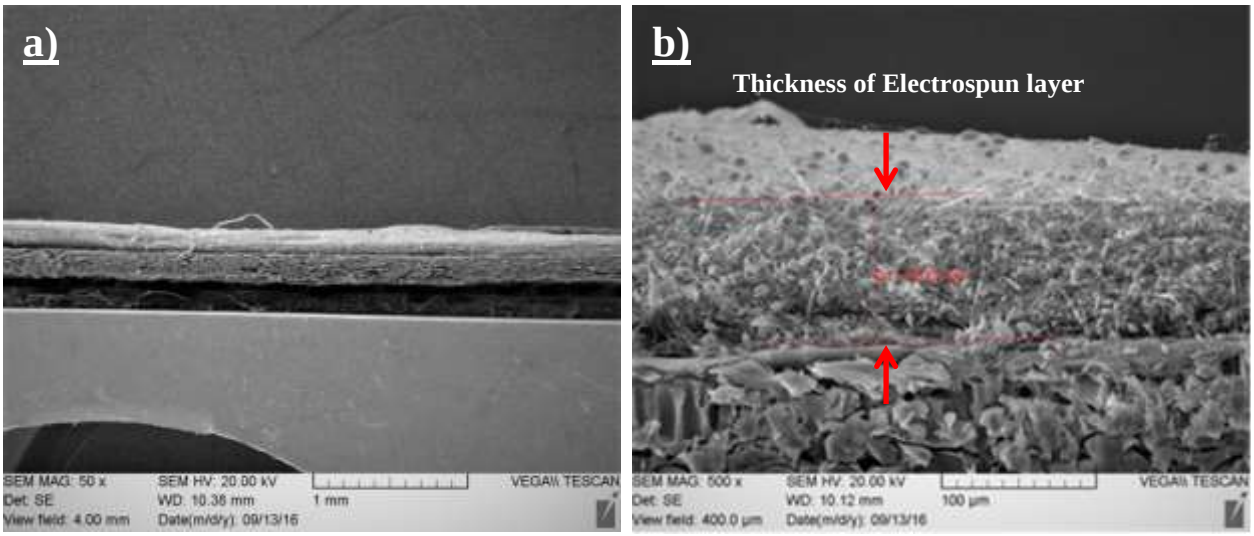

Figure 4. 14 Cross-sectional images of virgin EPES-250 membrane

As expected, the electrospun layer thickness increased with electrospinning time (Figure 4.15). This graph shows almost a nearly linear trend of increase for EPES-25 to EPES-250. However, the thickness was not uniform and varied along the cross sections of membrane, for all measured samples the EPES-250 had a higher thickness of electrospun layer compared to the other two EPES membranes.

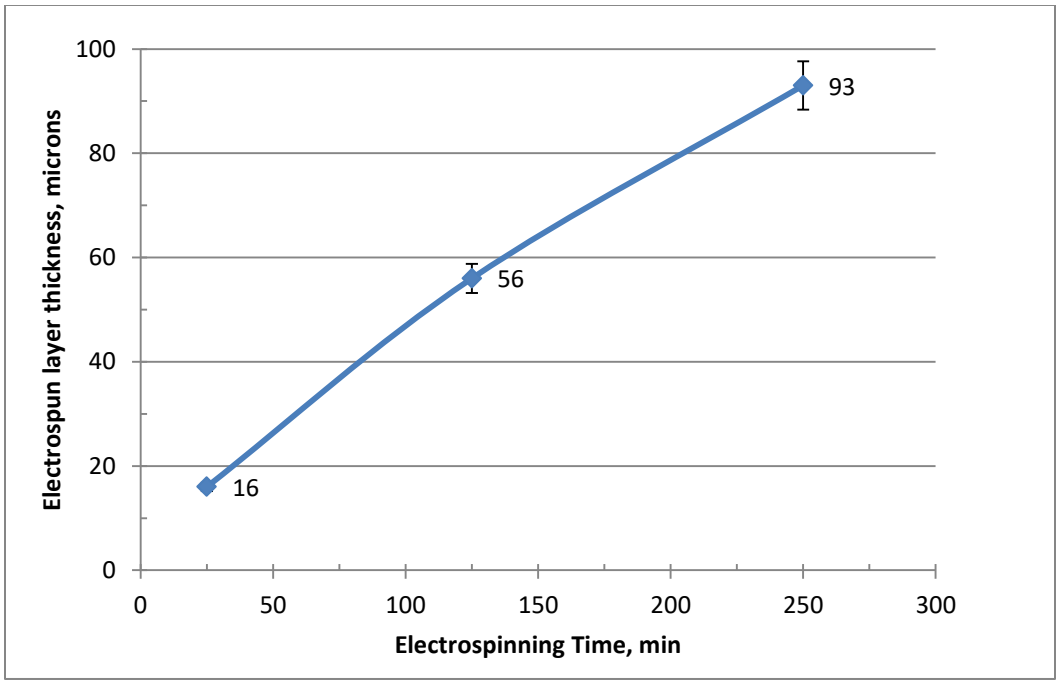

Figure 4.15 Membrane electrospun layer thickness versus electrospinning time

4.3.2 Contact angle measurements

Results of the contact angle measurements for the virgin membranes (i.e., before filtration and fouling) are summarized in Table 4.9. Measurements were performed at 20 locations and twice per location on the membrane surface.

Table 4. 9 Summary of contact angle measurements of the virgin membranes

	Contact angle (degree)			
	PES	**EPES-25**	**EPES- 125**	**EPES- 250**
Average*	62.7	85	109	110
Standard deviation	0.57	0.74	1.34	1.09

* Average of 20 measurements

Table 4.9 shows the measured contact angle of the PES membrane was approximately 63^{o}, this is close to the value of 58° cited for clean PES membrane by Kertesz et al. (2014). Since the angle is lower than 90^{o} and the membrane is considered as hydrophilic (Law, 2014). Zhao et al. (2011) also reported that pristine PES has a contact angle of around 75^{o}. Nguyen et al. (2007) measured the contact angle of commercial and lab-made PES membranes and reported contact angle values of around 80^{o}. In addition, Dang et al. (2006) reported a range of contact angle, 47- 67 ^{o} for the PES membranes they tested. Thus, the value measured in this study is reasonable.

The lower contact angle of the commercial PES membrane used in this study may be due to the additives used in its fabrication. Table 4.9 also shows that the contact angle

increases progressively from PES to EPES-125 as the electro-spinning period increases and then levels off (Figure 4.16).

Given that PVDF is more hydrophobic than PES, the electrospun membranes are expected to more hydrophobic than the commercial membrane tested. The data in Table 4.9 confirm this. Considering that both the electrospun nanofiber layer thickness and the contact angle increase, the flux would be expected to decrease with increasing nanofiber layer thickness. As discussed earlier, one of the hypotheses for the higher fluxes of the EPES membranes was that the larger pores and more hydrophobic characteristics of the nanofiber layer resulted in channeling of the flow through the membrane resulting less fluid friction and higher fluxes in EPES membranes.

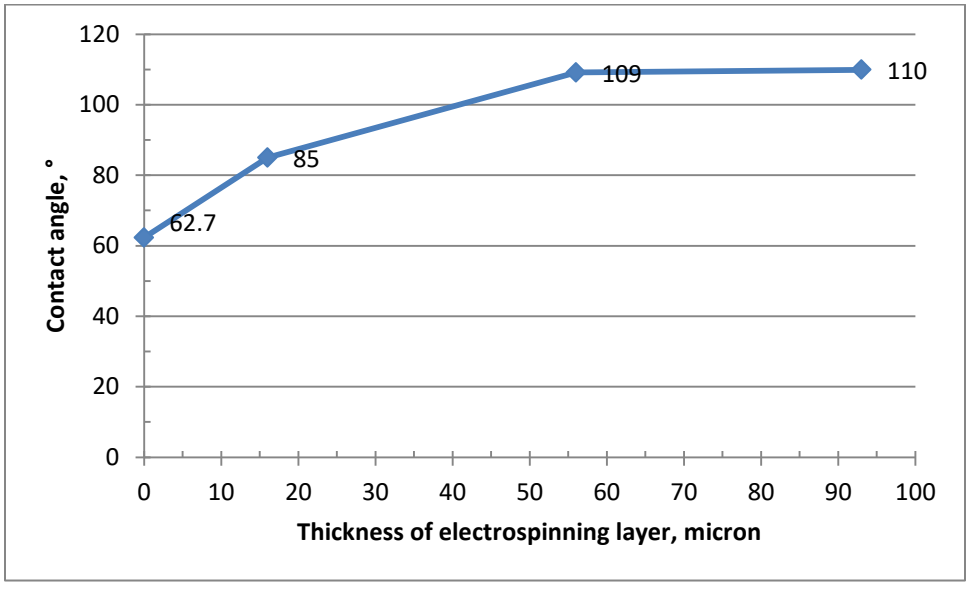

Figure 4. 16 Contact angle versus thickness of electrospun layer

4.3.3 Pore size and pore size distribution

The pore size distribution was determined based on the protein separation (removal) data. According to the method of Singh et al. (1998), based on the sieving mechanism, a straight line can be drawn through the selectivity (percent solute removal) versus solute diameter (or radius) plots on a log-normal probability graph. From the straight line, the mean pore diameter (or radius) is obtained as the solute size that corresponds to 50 % separation and the standard deviation from the ratio of the solute sizes corresponding to 84.13 % and 50 % separation.

In order to apply their method it is necessary to calculate the protein size. It can be calculated by first calculating the molecular diffusivity (D) of the proteins using the Young et al. (1980) equation which is based on the molecular weight of the proteins.

$$D = \frac{8.34\times10^{-8}T}{\eta M^{1/3}} \tag{4.6}$$

Where, T is absolute temperature, η is the viscosity of water and M is protein molecular weight (g mole^{-1}). It should be noted that the above empirical equation is based on g-cm-s system and therefore diffusivity D is obtained as cm^2 s^{-1}. Then, the molecular diffusivity can be substituted into the following Stokes equation to estimate the molecular radius of the proteins (Singh et al., 1997).

$$r = \frac{kT}{6\pi\eta D} \tag{4.7}$$

Where, k is the Boltzmann constant (1.38x10^{-23} J K^{-1}), η is the viscosity of water (Pa s) and D is the protein molecular diffusivity (m^2 s^{-1}). Also, the Stokes equation (4.7) is based on the SI system.

The molecular weight of the proteins utilized in the experiments, the estimated protein diffusivity in water (*D),* and the estimated protein radius, *r*, are summarized in Table 4.10.

Table 4. 10 Molecular weight, diffusivity and radius of protein

Protein	**Trypsin**	**Pepsin**	**Egg Albumin**	**BSA**
***M* (g mole^{-1})**	2300	34500	42700	67000
D **(m^2 s^{-1}) x 10^{10}**	2.122	0.8614	0.8023	0.6905
***r* (nm)**	1.156	2.848	3.057	3.552

When solute rejection, *R* (%), is plotted on the y-axis of the log-normal distribution graph y, the density of probability, is given by the following error function,

$$R(x) = \frac{2}{\sqrt{\pi}} \int_0^x e^{-t^2} dt \qquad (4.8)$$

While on the x axis, $x = ln\ r$.

The fluxes obtained from the filtration of the protein solutions were reported in Table 4.6. The corresponding solute rejection data from the Series 4 PES and EPES-250 membranes are summarized in Table 4.11. In addition, the values of "y" from equation 4.8 based on the percentage of separation of each protein for EPES- 250 membrane are extracted from the table presented in Appendix B. It is necessary to mention that data for pepsin was not included because it yielded irregularly low separation for both the PES and EPES- 250 membranes.

Table 4. 11 Protein rejection by Series 4 PES and EPES-250

Protein	**Trypsin (MW = 2300)**		**Pepsin (MW = 34500)**		**Egg Albumin (MW = 42700)**		**BSA (MW = 67000)**	
Membrane	**PES**	**EPES-250**	**PES**	**EPES-250**	**PES**	**EPES-250**	**PES**	**EPES-250**
Protein rejection (%)	85	82	-	-	98	92	96	99
y*		0.92		-		1.41		2.33

* y represents density of probability in normal distribution

As expected, for the PES membrane the solute separation increases progressively as the protein molecular weight increases from Trypsin to BSA, with an exception of Egg Albumin and BSA rejection. The removals by the PES and EPES membrane were similar. This implies that the solute removal by the EPES membrane was primarily controlled by the PES support layer with pores smaller than voids of electrospun layer; this was expected and also was observed in SEM images because pores cannot be seen on the surface of the virgin PES membrane while voids of the electrospun layer are visible. The

slight differences in the percent of removals reported in Table 4.11 are likely due to the analytical errors and differences among coupons tested.

Using the above protein rejection data, an attempt was made to determine the pore size and pore size distribution of EPES-250. A set of data y and x are given in Table 4.12, where y is based on the separation data of Trypsin, Egg Albumin and BSA by ESEP-250 given in Table 4.11.

Table 4.12 y and x obtained from the protein separation of Series 4 ESEP-250 and protein radius

	Trypsin	**Egg Albumin**	**BSA**
y, obtained by equation 4.8	0.92	1.41	2.33
x = ln r	0.15	1.12	1.27

The linear regression between y and x for the EPES-250 membrane data yields

$$y = 0.989x + 0.716 \qquad (4.9)$$

From equation 4.8, y = 0 and 1, correspond to R = 50 and 84.13 %, respectively. Then, by equation 4.9, for y= 0 and 1, x values were calculated as - 0.724 and 0.287, on an individual basis. Therefore, the average pore size was 0.485 nm and the upper bound of the normal distribution was 1.33 nm. Estimating standard deviation, 2.742, the lower bound of the normal distribution is 0.177 nm.

The pore size at the lower bound seems unreasonable because it is in the sub-nanometer range, but it can be concluded that the pore sizes are those of nano- to ultrafiltration membranes. Since the pore size of the electrospun nanofiber layer is larger than the proteins (see Figure 4.8 a), according to the protein rejection percent in Table 4.11, it can be concluded that the protein separation is primarily performed by the PES sublayer, except for BSA. The nanofiber layer does not affect the structure of the base membrane, as reported by Dobosz et al. (2017). The protein separations of EPES-250 membrane are slightly lower than those by the PES membrane presumably due to the concentration polarization occurring in the electro-spun nanofiber layer.

Another attempt to evaluate the pore size was made applying the following pore radius equation proposed by Kanagaraj et al. (2015).

$$Pore\ radius = 100 \times \frac{r}{R} \tag{4.10}$$

Where r is the Stokes radius (nm) of the solute and *R* is the percentage of solute rejection. Using this simple equation, pore radii for EPES- 250 are obtained as 1.38, 3.34 and 3.59 nm from Trypsin, Egg Albumin and BSA, respectively. Also, the pore size obtained by this method depends on the solute and is larger than the average pore radius obtained by Singh's method.

Chapter 5

Conclusions and recommendations

5.1 Conclusions

From the experimental results the following conclusions can be drawn:

1) The permeate flux of a commercial PES ultrafiltration membranes was enhanced by the coating of electro-spun PVDF nanofiber layer. It is hypothesized that the electrospun layer makes the modified PES stronger so that its pores deform less than those of the commercial PES membrane and/ or the larger pores of the hydrophobic electrospun layer channel the flow, resulting in less friction and higher fluxes in electrospun membranes.

2) The electro-spun nanofiber layer caused the fouling to be more severe than that for the PES substrate membrane, yet, the flux of the nanofiber-coated membrane remained higher than the pristine PES membrane during the 4h filtration period.

3) The Ottawa River water fouling of the PES substrate and nanofiber-coated membranes was irreversible whereas the fouling caused by the BSA solutions was reversible for the PES substrate membrane and irreversible for the nanofiber coated membrane.

4) The thickness of the nanofiber layer increased proportionally with the electro-spinning period.

5) The contact angle initially increased as the electro-spinning period was increased and levelled for the longest electrospinning periods.

6) The separation of protein solute was governed by the PES substrate membrane even after the coating of the nanofiber layer.

7) Based on the rejection of protein solute of various molecular sizes, it was confirmed that the pore size and pore size distribution of electrospun PES (EPES) membranes are in the ultrafiltration/nanofiltration range.

5.2 Recommendations

The following recommendations are made for the future work:

1) Longer filtration/fouling tests in terms of time should be carried out with OR Water as well as with protein solutions in order to investigate the flux reduction trend and fouling of EPES membranes and commercial PES over the time.

2) It is recommended that the electrospun membrane be also evaluated for the filtration of solutions of hydrophilic macromolecular solutes, such as sodium alginate that is a microbial polysaccharide as a potential foulant for drinking water treatment.

3) The unexpected behaviour of EPES-125 (lower permeate fluxes than the other electrospun membranes) should be confirmed and explained by applying more related experiments and using different foulants.

4) Prepare and test membranes with electrospun layers of different polymers to determine the effect of hydrophobicity of the polymer on the flux enhancement.

5) Investigatation of alternative cleaning methods to achieve higher flux recoveries for the EPES membranes.

References:

Al-Bastaki, N., & Abbas, A. (2001). Use of fluid instabilities to enhance membrane performance: A review. *Desalination*, 136(1-3), 255-262.

Balmann, H., Nobrega,R., Aimar, P., & Sanchez, V. (1989). Transfer of dextran through ultrafiltration membranes: A study of rejection data analyzed by gel formation chromatography. *Journal of Membrane Science*, 45, 17-36.

Baker, R. W. (2012). Membrane technology and applications. Published by John Wiley and Sons, Newark, NJ, 592.

Belfort, G., Davis, R. H., & Zydney, A. L. (1994). The behaviour of suspensions and macromolecular solutions in crossflow microfiltration. *Journal of Membrane Science,* 96, 1-58.

Bjorge, D., Daels, N., De Vrieze, S., Dejans, P., Van Camp, T., Audenaert, W., Westbroek, Ph., De Clerck, K., Boeckaert, Ch., & Van Hulle, S. W. H. (2010). Initial testing of electrospun nanofibre filters in water filtration applications. *Water SA*, 36(1), 151-156.

Buonomenna, M. G., Choi, S., Galiano, F., & Drioli, E. (2011). Membranes prepared via phase inversion. Membranes for Membrane reactors: Preparation, Optimization and Selection. Published by John Wiley and Sons, Newark, N J, 476–489. https://doi.org/10.1002/9780470977569.ch21

Chen, A., Fan, Q., & Tian, Q. (2013). Study on dynamic of ultrafiltration membrane materials preparing and used in drinking water treatment, *International Journal of Environmental Science and Development*, 4(4), 383-385.

Chen, V., Mansouri , J., & Charlton, T. (2010). Biofouling in membrane systems , membrane for water treatment, Published by Wiley- VCH, Verleg, Weinheim, Germany, 250.

Contreras, A., Kim, A., & Li, Q. (2009). Combined fouling of nanofiltration membranes: Mechanisms and effect of organic matter. *Journal of Membrane Science*, 327(1-2), 87-95.

Crittenden, J. C., Trussell, R. R., Hand, D. W., Howe, K. J., & Tchobanoglous, G. (2012). MWH's water treatment : principles and design. (Third ed.). Published by John Wiley and Sons, Hoboken, NJ, 1901

Dang, H., Narbaitz, R.M., Matsuura, T., & Khulbe, K. (2006). A comparison of commercial and experimental ultrafiltration membranes via surface property analysis and fouling tests. *Water Quality Research Journal of Canada*, 41(1), 84-93.

Dobosz, K., Kuo-Leblanc, C., Martin, T., & Schiffman, J. (2017). Ultrafiltration membranes enhanced with electrospun nanofibers exhibit improved flux and fouling resistance. *Industrial and Engineering Chemistry Research*, 56(19), 5724-5733.

Duranceau, S. (2001). Membrane practices for water treatment. Published by AWWA, Denver,Co, 589.

Edzwald, J. K. (2011). Water quality & treatment: a handbook on drinking water. (Sixth ed.) Published by McGraw-Hill Education, New York, NY, 1696.

Efome, J., Rana, D., Matsuura, T., & Lan, C. (2016). Enhanced performance of PVDF nanocomposite membrane by nanofiber coating: A membrane for sustainable desalination through MD. *Water Research,* 89, 39-49.

Fane, A., & Fell, C. (1987). A review of fouling and fouling control in ultrafiltration. *Desalination,* 62(C), 117-136.

Fang, X., Li, J., Li, X., Sun, X., Shen, J., Han, W., & Wang, L. (2015). Polyethyleneimine, an effective additive for polyethersulfone ultrafiltration membrane with enhanced permeability and selectivity. *Journal of Membrane Science*, 476, 216-223.

Feng, C., Khulbe, K., Matsuura, T., Tabe, S., & Ismail, A. (2013). Preparation and characterization of electro-spun nanofiber membranes and their possible applications in water treatment. *Separation and Purification Technology*, 102, 118-135.

Field, R. (2010). Fundamentals of fouling. In R. Field, Membranes for water treatment (Vol. 4, pp. 1-23). Published by WILEY-VCH Verlag GmbH & Co. KGaA Weinheim, Weinheim, Germany, 1-23.

Foley, G. (2011). Adapted from PA website, dated November 2005, and National drinking water clearing house website, dated March 1999. Membrane filtration: A problem solving approach with MATLAB. Membrane filtration: A problem solving approach with MATLAB, Chapter 19, Published by Cambridge University Press, Cambridge, England, 327.

Gatenholm, P., Fell, C., & Fane, A. (1988). Influence of the membrane structure on the composition of the deposit-layer during processing of microbial suspensions. *Desalination*, 70(1-3), 363-378.

Geise, G., Lee, H.-S., Miller, D., Freeman, B., Mcgrath, j., & Paul, D. R. (2010). Water Purificationby by Membranes: The Role of Polymer science. *Polymer Science,* 48, 1685- 1718.

Giaouris, E., Chorianopoulos, N., Skandamis, P., & Nychas, G. (2012). World ' s largest Science , technology & medicine open access book, Salmonella: A dangerous foodborne pathogen, Published by InTech, Rijeka, Croatia, 450.

Gopal, R., Kaur, S., Ma, Z., Chan, C., Ramakrishna, S., & Matsuura, T. (2006). Electrospun nanofibrous filtration membrane. *Journal of Membrane Science*, 281(1-2), 581-586.

Huang, Z., Zhang, Y., Kotaki, M., & Ramakrishna, S. (2003). A review on polymer nanofibers by electrospinning and their applications in nanocomposites. *Composites Science and Technology*, 63(15), 2223-2253.

Idris, A., Mat Zain, N., & Noordin, M. (2007). Synthesis, characterization and performance of asymmetric polyethersulfone (PES) ultrafiltration membranes with polyethylene glycol of different molecular weights as additives. *Desalination*, 207(1-3), 324-339.

Introduction to charge retention on electrospun fibers. (2014). Retrieved (2014) from electrospintech.com/introcharge.html

Jamshidi Gohari, R., Lau, W., Matsuura, T., & Ismail, A. (2013). Effect of surface pattern formation on membrane fouling and its control in phase inversion process. *Journal of Membrane Science*, 446, 326-331.

Jermann, D., Pronk, W., Meylan, S., & Boller, M. (2007). Interplay of different NOM fouling mechanisms during ultrafiltration for drinking water production. *Water Research*, 41(8), 1713-1722.

Kanagaraj, P., Neelakandan, S., & Nagendran, A. (2014). Poly(ether imide) membranes modified with charged surface-modifying macromolecule - Its performance characteristics as ultrafiltration membranes. *Journal of Applied Polymer Science*, 131(11), 1-8.

Kertész, S., Veszprémi, Á., László, Z., Csanádi, J., Keszthelyi-Szabó, G., & Hodúr, C. (2015). Investigation of module vibration in ultrafiltration. *Desalination and Water Treatment*, 55(10), 2836-2842.

Khamforoush, M., Pirouzram, O., & Hatami, T. (2015). The evaluation of thin film composite membrane composed of an electrospun polyacrylonitrile nanofibrous mid-layer for separating oil-water mixture. *Desalination*, 359, 14-21.

Khayet, M., & Matsuura, T. (2011). Membrane distillation: Principles and applications. Published by Elsevier, Amsterdam, Netherland, 512.

Khulbe, K. (2008). 2 Synthetic membranes for membrane processes. Synthetic polymeric membranes: Published by Springer-Verlag, Berlin, Germany, 5-18.

Ladewig, B., & Al-Shaeli, M. (2017). Fundamentals of Membrane Processes. Published by Springer Nature Singapore Pte Ltd., Singapore, Singapore, 13-37.

Lau, W. J., & Ismail, A. F. (2011). Progress in interfacial polymerization technique on composite membrane preparation. *International proceedings of chemical, biological and environmental engineering*, 17, 173–177.

Law, K.-Y. (2014). Definitions for hydrophilicity, hydrophobicity, and superhydrophobicity: getting the basics right. *The Journal of Physical Chemistry Letters*, 5(4), 686-688.

Le-Clech, P., Chen, V., & Fane, T. (2006). Fouling in membrane bioreactors used in wastewater treatment. *Journal of Membrane Science*, 284(1-2), 17-53.

Le, N. L., & Nunes, S. P. (2016). Materials and membranes technologies for water energy sustainability. *Journal of Sustainable Materials and Technologies, 7, 1-28.*

Lee, J.-W., Jung, J. , Cho, Y. H., Yadav, S. K., Baek, K. Y., Park, H. B.,Hong, S. M., & Koo, C. M. (2014). Fouling-tolerant nanofibrous polymer membranes for water treatment. ACS *Applied Materials & Interfaces*, 6(16), 14600-14607.

Low, Z. X., Liu, Q., Shamsaei, E., Zhang, X., & Wang, H. (2015). Preparation and characterization of thin-film composite membrane with nanowire-modified support for forward osmosis process. *Membranes*, *5*(1), 136–149. https://doi.org/10.3390/membranes5010136

Maruf, S., Wang, L., Greenberg, A., Pellegrino, J., & Ding, Y. (2013). Use of nanoimprinted surface patterns to mitigate colloidal deposition on ultrafiltration membranes. *Journal of Membrane Science*, 428, 598-607.

Montgomery, D. C., & Runger G., C. (2011). Applied statistics and probability for engineers (fifth ed.). Published by John Wiley & Sons, Hoboken, NJ, 811.

Mosqueda-Jimenez, D., Narbaitz, R. M., & Matsuura, T. (2004). Membrane fouling test: Apparatus evaluation. *Journal of Environmental Engineering-ASCE,* 130(1), 90-99.

Muthukumaran, S., Kentish, S., Lalchandani, S., Ashokkumar, M., Mawson, R., Stevens, G., & Grieser, F. (2005). The optimisation of ultrasonic cleaning procedures for dairy fouled ultrafiltration membranes. *Ultrasonics Sonochemistry*, 12(1-2 SPEC. ISS.), 29-35.

Muthukumaran, S., Yang, K., Seuren, A., Kentish, S., Ashokkumar, M., Stevens, G., & Grieser, F. (2004). The use of ultrasonic cleaning for ultrafiltration membranes in the dairy industry. *Separation and Purification Technology*, 39(1-2 SPEC. ISS.), 99-107.

Nakao, S., Osada, H., Kurata, H., Tsuru, T., & Kimura, S. (1988). Separation of proteins by charged ultrafiltration membranes. *Desalination*, 70(1-3), 191-205.

Nasreen, S., Sundarrajan, S., Nizar, S., Balamurugan, R., & Ramakrishna, S. (2013). Advancement in electrospun nanofibrous membranes modification and their application in water treatment. *Membranes*, 3(4), 266-284.

Naylor, T. V. (1996). *Polymer* membranes: materials, structures and separation performance. Published by iSmithers Rapra Technology Limited, Shropshire, England, 136.

Nguyen, A., Narbaitz, R. M., & Matsuura, T. (2007). Impacts of hydrophilic membrane additives on the ultrafiltration of river water. *Journal of Environmental Engineering-ASCE*, 133(5), 515-522.

Olson, W., Bethel, G., & Parker, C. (1977). Rapid delipidation of and Particulate removal from human serum by membrane filtration in a tangential flow system. *Preparative Biochemistry*, 7(5), 333-343.

Pezeshk, N. (2010). Modified PVDF ultrafiltration flat sheet membranes for water treatment. MASc thesis, dept. of Civil Engineering, University of Ottawa, Ottawa, Canada.

Pezeshk, N., Rana, D., Narbaitz, R. M., & Matsuura, T. (2012). Novel modified PVDF ultrafiltration flat-sheet membranes. *Journal of Membrane Science*, 389, 280-286.

Pearce, G. (2011). UF/MF Membrane water treatment: Principles and design. Published by Water Treatment Academy, Bangkok, Thailand, 387.

Pinnau, I. (1994). Recent advances in the formation of ultrathin polymeric membranes for gas separations. *Section title: Plastics fabrication and uses*, 5(1), 733-744.

Pinnau, I., & Freeman, B. (2000). Membrane formation and modification (Vol. 744). Published by ACS publications, Washington, DC, 361.

Rana, D., & Matsuura, T. (2010). Surface modifications for antifouling membranes. *Chemical Reviews*, 110(4), 2448-2471.

Romijn, D., Brink, L. (1990). Reducing the protein fouling of polysulfone surfaces and polysulfone ultrafiltration membranes : Optimization of the type of presorbed layer. *Desalination*, 78(2), 209-233.

Schaefer, A. I.; Fane, A. G., Waite, T. D. (2005). Nanofiltration : principles and applications. Published by Elesevier, Oxford, England, 620.

Shi, X., Tal, G., Hankins, N., & Gitis, V. (2014). Fouling and cleaning of ultrafiltration membranes: A review. *Journal of Water Process Engineering*, 1, 121-138.

Singh, S., Khulbe, K., Matsuura, T., & Ramamurthy, P. (1998). Membrane characterization by solute transport and atomic force microscopy. *Journal of Membrane Science*, 142(1), 111-127.

Sourirajan, S., & Matsuura, T. (1985). Reverse osmosis/ultrafiltration process principles. Published by National Research Council of Canada, Ottawa, 1113.

Tanny, G., Hauk, D., & Merin, U. (1982). Biotechnical applications of a pleated crossflow microfiltration module. *Desalination*, 41(3), 299-312.

Tombácz, E., & Szekeres, M. (2006). Surface charge heterogeneity of kaolinite in aqueous suspension in comparison with montmorillonite. *Applied Clay Science*, 34(1-4), 105-124.

Tombácz, E., Libor, Z., Illés, E., Majzik, A., & Klumpp, E. (2004). The role of reactive surface sites and complexation by humic acids in the interaction of clay mineral and iron oxide particles. *Organic Geochemistry*, 35(3), 257-267.

Ulbricht, M. (2006). Advanced functional polymer membranes. Polymer, 47(7), 2217-2262.

Villaluenga, J. P. G., Khayet, M., Godino, P., Seoane, B., & Mengual J. I. (2005). Analysis of the membrane thickness effect on the pervaporation separation of methanol/ methyl tertiary butyl ether mixtures. *Journal of Separation and Purification Technology*, 47(1-2), 80- 87

Wang, D., Lu, Q., Wei, M., & Guo, E. (2017). Electrospinning of flux-enhanced chitosan–poly(lactic acid) nanofiber mats as a versatile platform for oil–water separation. *Journal of Applied Polymer Science*, 135(6), 1-7.

Wang, R., Liu, Y., Li, B., Hsiao, B., & Chu, B. (2012). Electrospun nanofibrous membranes for high flux microfiltration. *Journal of Membrane Science*, 392-393, 167-174.

Xu, B. (2015). Improved membrane pretreatment by flotation. MASc thesis, dept. of Civil Engineering, University of Ottawa, Ottawa, Canada.

Yoon, K., Hsiao, B., & Chu, B. (2009). Formation of functional polyethersulfone electrospun membrane for water purification by mixed solvent and oxidation processes. *Polymer*, 50(13), 2893-2899.

Young, M., Carroad, P., & Bell, R. (1980). Estimation of diffusion coefficients of proteins. *Biotechnology and Bioengineering*, 22(5), 947-955.

Zhang, L., Chowdhury, G., Feng, C., Matsuura, T., & Narbaitz, R. M. (2003). Effect of surface-modifying, macromolecules and membrane morphology on fouling of polyethersulfone ultrafiltration membranes. *Journal of Applied Polymer Science*, 88(14), 3132-3138.

Zhao, W., Huang, J., Fang, B., Nie, S., Yi, N., Su, B., Li, H., & Zhao, C. (2011). Modification of polyethersulfone membrane by blending semi-interpenetrating network polymeric nanoparticles. *Journal of Membrane Science*, 369(1-2), 258-266.

Zhao, Y.-J., Wu, K.-F., Wang, Z.-J., Zhao, L., & Li, S.-S. (2000). Fouling and cleaning of membrane - a literature review. *Journal of Environmental Sciences*, 12(2), 241-251.

APPENDIX A

Figure A.1 shows the PWP of the PES membrane that was electrospun with only DMAc solvent and without polymer to create nanofibers. This has been performed to establish whether the solvent used in the eletrospinning could be damaging the commercial PES membrane surface and thus increase its flux. Figure illustrates that the values of flux or PWP are almost the same as PES.

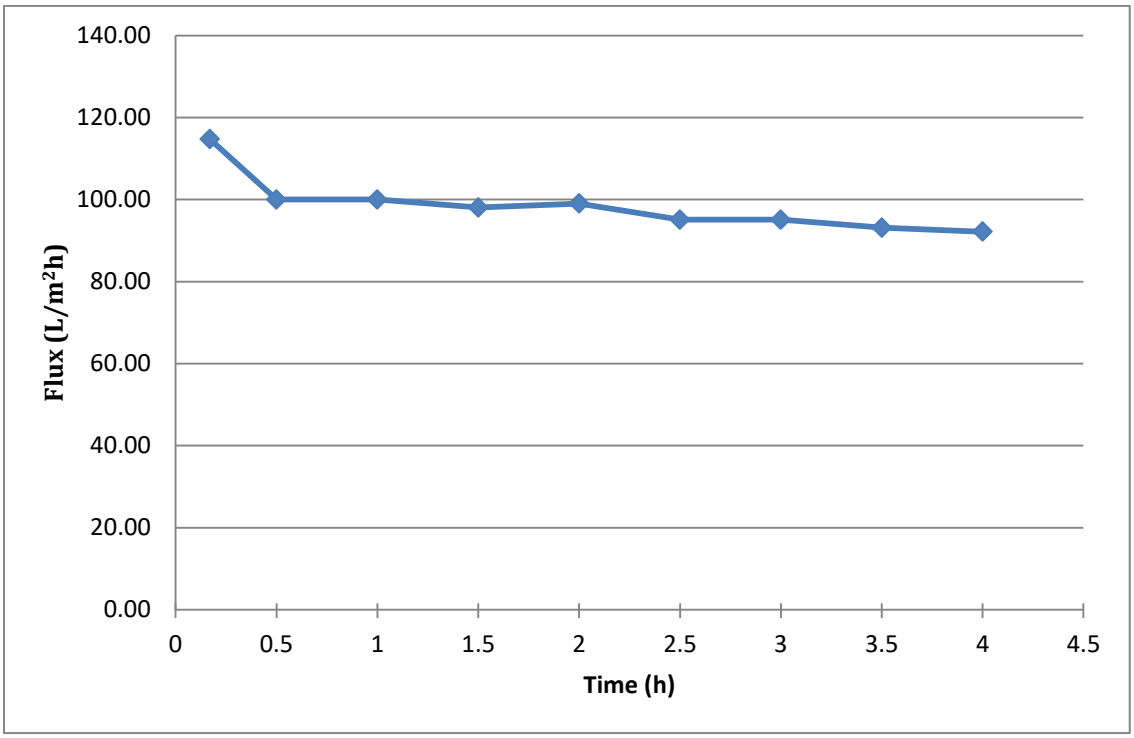

Figure A. 1 PWP for electrospun PES with DMAc solvent

APPENDIX B

Tables B.1 and B.2 present standard normal distribution, y, based on the percentage of separation (Montgomery & Runger, 2011).

Table B. 1 Standard Normal Distribution

STANDARD NORMAL DISTRIBUTION: Table Values Represent AREA to the LEFT of the Z score.

Z	.00	.01	.02	.03	.04	.05	.06	.07	.08	.09
-3.9	.00005	.00005	.00004	.00004	.00004	.00004	.00004	.00004	.00003	.00003
-3.8	.00007	.00007	.00007	.00006	.00006	.00006	.00006	.00005	.00005	.00005
-3.7	.00011	.00010	.00010	.00010	.00009	.00009	.00008	.00008	.00008	.00008
-3.6	.00016	.00015	.00015	.00014	.00014	.00013	.00013	.00012	.00012	.00011
-3.5	.00023	.00022	.00022	.00021	.00020	.00019	.00019	.00018	.00017	.00017
-3.4	.00034	.00032	.00031	.00030	.00029	.00028	.00027	.00026	.00025	.00024
-3.3	.00048	.00047	.00045	.00043	.00042	.00040	.00039	.00038	.00036	.00035
-3.2	.00069	.00066	.00064	.00062	.00060	.00058	.00056	.00054	.00052	.00050
-3.1	.00097	.00094	.00090	.00087	.00084	.00082	.00079	.00076	.00074	.00071
-3.0	.00135	.00131	.00126	.00122	.00118	.00114	.00111	.00107	.00104	.00100
-2.9	.00187	.00181	.00175	.00169	.00164	.00159	.00154	.00149	.00144	.00139
-2.8	.00256	.00248	.00240	.00233	.00226	.00219	.00212	.00205	.00199	.00193
-2.7	.00347	.00336	.00326	.00317	.00307	.00298	.00289	.00280	.00272	.00264
-2.6	.00466	.00453	.00440	.00427	.00415	.00402	.00391	.00379	.00368	.00357
-2.5	.00621	.00604	.00587	.00570	.00554	.00539	.00523	.00508	.00494	.00480
-2.4	.00820	.00798	.00776	.00755	.00734	.00714	.00695	.00676	.00657	.00639
-2.3	.01072	.01044	.01017	.00990	.00964	.00939	.00914	.00889	.00866	.00842
-2.2	.01390	.01355	.01321	.01287	.01255	.01222	.01191	.01160	.01130	.01101
-2.1	.01786	.01743	.01700	.01659	.01618	.01578	.01539	.01500	.01463	.01426
-2.0	.02275	.02222	.02169	.02118	.02068	.02018	.01970	.01923	.01876	.01831
-1.9	.02872	.02807	.02743	.02680	.02619	.02559	.02500	.02442	.02385	.02330
-1.8	.03593	.03515	.03438	.03362	.03288	.03216	.03144	.03074	.03005	.02938
-1.7	.04457	.04363	.04272	.04182	.04093	.04006	.03920	.03836	.03754	.03673
-1.6	.05480	.05370	.05262	.05155	.05050	.04947	.04846	.04746	.04648	.04551
-1.5	.06681	.06552	.06426	.06301	.06178	.06057	.05938	.05821	.05705	.05592
-1.4	.08076	.07927	.07780	.07636	.07493	.07353	.07215	.07078	.06944	.06811
-1.3	.09680	.09510	.09342	.09176	.09012	.08851	.08691	.08534	.08379	.08226
-1.2	.11507	.11314	.11123	.10935	.10749	.10565	.10383	.10204	.10027	.09853
-1.1	.13567	.13350	.13136	.12924	.12714	.12507	.12302	.12100	.11900	.11702
-1.0	.15866	.15625	.15386	.15151	.14917	.14686	.14457	.14231	.14007	.13786
-0.9	.18406	.18141	.17879	.17619	.17361	.17106	.16853	.16602	.16354	.16109
-0.8	.21186	.20897	.20611	.20327	.20045	.19766	.19489	.19215	.18943	.18673
-0.7	.24196	.23885	.23576	.23270	.22965	.22663	.22363	.22065	.21770	.21476
-0.6	.27425	.27093	.26763	.26435	.26109	.25785	.25463	.25143	.24825	.24510
-0.5	.30854	.30503	.30153	.29806	.29460	.29116	.28774	.28434	.28096	.27760
-0.4	.34458	.34090	.33724	.33360	.32997	.32636	.32276	.31918	.31561	.31207
-0.3	.38209	.37828	.37448	.37070	.36693	.36317	.35942	.35569	.35197	.34827
-0.2	.42074	.41683	.41294	.40905	.40517	.40129	.39743	.39358	.38974	.38591
-0.1	.46017	.45620	.45224	.44828	.44433	.44038	.43644	.43251	.42858	.42465
-0.0	.50000	.49601	.49202	.48803	.48405	.48006	.47608	.47210	.46812	.46414

Table B. 2 Standard Normal Distribution

STANDARD NORMAL DISTRIBUTION: Table Values Represent AREA to the LEFT of the Z score.

Z	.00	.01	.02	.03	.04	.05	.06	.07	.08	.09
0.0	.50000	.50399	.50798	.51197	.51595	.51994	.52392	.52790	.53188	.53586
0.1	.53983	.54380	.54776	.55172	.55567	.55962	.56356	.56749	.57142	.57535
0.2	.57926	.58317	.58706	.59095	.59483	.59871	.60257	.60642	.61026	.61409
0.3	.61791	.62172	.62552	.62930	.63307	.63683	.64058	.64431	.64803	.65173
0.4	.65542	.65910	.66276	.66640	.67003	.67364	.67724	.68082	.68439	.68793
0.5	.69146	.69497	.69847	.70194	.70540	.70884	.71226	.71566	.71904	.72240
0.6	.72575	.72907	.73237	.73565	.73891	.74215	.74537	.74857	.75175	.75490
0.7	.75804	.76115	.76424	.76730	.77035	.77337	.77637	.77935	.78230	.78524
0.8	.78814	.79103	.79389	.79673	.79955	.80234	.80511	.80785	.81057	.81327
0.9	.81594	.81859	.82121	.82381	.82639	.82894	.83147	.83398	.83646	.83891
1.0	.84134	.84375	.84614	.84849	.85083	.85314	.85543	.85769	.85993	.86214
1.1	.86433	.86650	.86864	.87076	.87286	.87493	.87698	.87900	.88100	.88298
1.2	.88493	.88686	.88877	.89065	.89251	.89435	.89617	.89796	.89973	.90147
1.3	.90320	.90490	.90658	.90824	.90988	.91149	.91309	.91466	.91621	.91774
1.4	.91924	.92073	.92220	.92364	.92507	.92647	.92785	.92922	.93056	.93189
1.5	.93319	.93448	.93574	.93699	.93822	.93943	.94062	.94179	.94295	.94408
1.6	.94520	.94630	.94738	.94845	.94950	.95053	.95154	.95254	.95352	.95449
1.7	.95543	.95637	.95728	.95818	.95907	.95994	.96080	.96164	.96246	.96327
1.8	.96407	.96485	.96562	.96638	.96712	.96784	.96856	.96926	.96995	.97062
1.9	.97128	.97193	.97257	.97320	.97381	.97441	.97500	.97558	.97615	.97670
2.0	.97725	.97778	.97831	.97882	.97932	.97982	.98030	.98077	.98124	.98169
2.1	.98214	.98257	.98300	.98341	.98382	.98422	.98461	.98500	.98537	.98574
2.2	.98610	.98645	.98679	.98713	.98745	.98778	.98809	.98840	.98870	.98899
2.3	.98928	.98956	.98983	.99010	.99036	.99061	.99086	.99111	.99134	.99158
2.4	.99180	.99202	.99224	.99245	.99266	.99286	.99305	.99324	.99343	.99361
2.5	.99379	.99396	.99413	.99430	.99446	.99461	.99477	.99492	.99506	.99520
2.6	.99534	.99547	.99560	.99573	.99585	.99598	.99609	.99621	.99632	.99643
2.7	.99653	.99664	.99674	.99683	.99693	.99702	.99711	.99720	.99728	.99736
2.8	.99744	.99752	.99760	.99767	.99774	.99781	.99788	.99795	.99801	.99807
2.9	.99813	.99819	.99825	.99831	.99836	.99841	.99846	.99851	.99856	.99861
3.0	.99865	.99869	.99874	.99878	.99882	.99886	.99889	.99893	.99896	.99900
3.1	.99903	.99906	.99910	.99913	.99916	.99918	.99921	.99924	.99926	.99929
3.2	.99931	.99934	.99936	.99938	.99940	.99942	.99944	.99946	.99948	.99950
3.3	.99952	.99953	.99955	.99957	.99958	.99960	.99961	.99962	.99964	.99965
3.4	.99966	.99968	.99969	.99970	.99971	.99972	.99973	.99974	.99975	.99976
3.5	.99977	.99978	.99978	.99979	.99980	.99981	.99981	.99982	.99983	.99983
3.6	.99984	.99985	.99985	.99986	.99986	.99987	.99987	.99988	.99988	.99989
3.7	.99989	.99990	.99990	.99990	.99991	.99991	.99992	.99992	.99992	.99992
3.8	.99993	.99993	.99993	.99994	.99994	.99994	.99994	.99995	.99995	.99995
3.9	.99995	.99995	.99996	.99996	.99996	.99996	.99996	.99996	.99997	.99997